Click to see Slides of Oral Presentation

Magnetic and Radiometric Signatures in Soils above Hydrocarbon Accumulations, Toqui-Toqui and Mana Fields, Tolima, Colombia*

Henry M. Martínez-Gómez[1] and José-María Jaramillo M[2]

Search and Discovery Article #42046 (2017)**
Posted April 3, 2017

*Adapted from extended abstract based on oral presentation given at AAPG International Conference and Exhibition, Barcelona Spain, April 3-6, 2016

[1]Universidad de los Andes (hm.martinez57@uniandes.edu.co)
[2]Gmas Lab (jjaramillo@gmaslab.com)

Abstract

Diagenetic processes are significantly influenced by the redox conditions within the environment they take place. Long-term leakage of hydrocarbons, as well as seepage (macro or micro), can set up near-surface oxidation-reduction zones that favor chemical and mineralogical changes in soils, which produces an anomalous concentration of magnetic and radiometric minerals that can be measured with geophysical field instruments. Magnetic Field Strength and Gamma-Radiation data, as well as soil samples, were acquired on Toqui-Toqui and Maná oil fields, a hydrocarbon deposit in the Upper Magdalena Valley in Colombia, and a relationship between each of them was found. The contour maps of Gamma-Radiation measurements correspond in their highest values with the western border of Toqui-Toqui and Maná oil fields because there is where the reduction of soluble U^{6+} takes place, while the highest values of the Magnetic Field Strength are correlated with the location of some hydrocarbon productive areas inferred from the productive wells data and pointed out by the vertical derivatives of the Magnetic Field Strength.

Although local geological information does not correspond to the geophysical interpretation, the identification of important features of the oil fields structure was possible by using the Analytic Signal technique. Soil samples corresponding to the locations with the 5 highest and the 5 lowest Gamma-Radiation values were analyzed. Intermediate volcanic rocks have been determined to be the parental material of the soils by FUS-ICP and ICP-MS analyses, and some alteration features attributed to diagenetic processes have been identified. X-Ray Diffraction analysis shows the typical mineral association of andesitic rocks from the Central Cordillera of Colombia (northern Andes), but also exhibits the presence of diagenetic minerals which does not relate to the parental material and neither to the local geology: Ferroan-Dolomite, Siderite, and Elemental-Composition-Magnetite, which was differentiated from Titanium-Magnetite from the volcanic activity of the zone. A mineral that correlates with the Gamma-Ray measurements was not identified, so it is proposed to be caused by Authigenic-Uraninite in proportions

less than the detection limit of XRD, since this is consistent with the geophysical and chemical data. This study was made in a locality with known hydrocarbon presence, but it can be utilized in low-cost exploration and prospect evaluation as well.

Introduction

Surface manifestations of hydrocarbon seepage are affected directly or indirectly by bacteria and other microbes' activities. The microbial activity over some time span lead to the development of near surface oxidation-reduction zones, which favor the formation of mineralogical changes. The surface expression of hydrocarbon-induced alteration of soils and sediments can take many forms, which include: microbiological anomalies and the formation of "paraffin dirt"; mineralogical changes such as the formation of calcite, pyrite, uraninite, elemental sulfur, and magnetic iron oxides and sulfides; bleaching of red beds; clay mineral alteration; electrochemical changes; Gamma radiation anomalies; and biogeochemical and geobotanical anomalies (Schumacher, 1996). This alteration is so complex it has led to the development of very varied exploration methods such as soil carbonate methods, magnetic and electrical methods, radioactivity-based methods, and remote sensing methods. Schumacher (1996), in his overview of the major hydrocarbon-induced changes affecting soils and sediments, highlighted the importance of a scientifically development of these methods and a rigorous understanding of the factors dominating these processes, so they can be used for a successful surface hydrocarbon exploration.

The bacterial oxidation of light hydrocarbons and its influence in the pH and Eh of the surrounding environment produces changes in the stability fields of the different mineral species, which result in the precipitation or solution and remobilization of various minerals and elements, so the soils above leaking hydrocarbon accumulations become significantly and measurably different from the geological environment (Pirson, 1969; Oehler and Sternberg, 1984; Price, 1986; Schumacher, 1996). The surface alteration zone, which has been described empirically, can range from subtle biogeochemical anomalies, such as in Wyoming's Recluse field (Dalziel and Donovan, 1980; Schumacher, 1996), to hydrocarbon-induced diagenetic aureoles (HIDAs) described from the Cement Field area of Oklahoma (Donovan, 1974; Lilburn and Al-Shaieb, 1983, 1984; Schumacher, 1996), including the bleached ferric iron from the wall rock, described by Everett et al. (2002), of the Pliocene La Vela Formation on Venezuela's Falcon coast.

Early Observations

Features such as seeps, 'paraffin dirt', saline or sulfurous waters, surface mineralization, and topographic highs, have been correlated with productive areas since the earliest days of petroleum exploration, and Schumacher (1996) made a compilation of the most relevant observations.

In early observations Sawtelle (1936) reported those features as instrumental in the discovery of about 70% of American Gulf Coast oil fields. Harris (1908) reported the presence of pyrite and other sulfides in strata overlying oil fields associated with salt domes in Louisiana. Reeves (1922) observed the discoloration of surface red beds in the Cement field area of southwestern Oklahoma and noted the intense carbonate cementation over the crest of the Cement structure. Thompson (1933) observed that sulfur and pyrite are commonly associated with oil accumulations, and reported that in the presence of hydrocarbon gases, gypsum and anhydrite are replaced by limestone in salt dome cap rocks in the Persian Gulf-Iraq oil belt. He also described another of the common alteration products found in Persia known as Gach-i-turush, an

association of seepage petroleum, gypsum, jarosite, and sulfur caused by the interaction of petroleum with evaporites. McDermott (1940) and Rosaire (1940) reported the occurrence of secondary mineralization such as soil carbonates, caliche, and silicification in the vicinity of some Texas oil fields.

Feely and Kulp (1957) demonstrated that the sulfur present in the cap rocks of gulf Coast salt domes originated by bacterial action on the anhydrite and that calcite replaced anhydrite as a result of bacterial oxidation of petroleum. Even though the close association between hydrocarbon accumulations and surface mineralization or discoloration has long been noted, detailed research started only since the 1970s. Donovan (1974) described for the first time the complex chemical and mineralogical changes observed in red beds over Oklahoma oil fields (Schumacher, 1996). More recent studies have documented these and other changes and discuss the processes involved (Oehler and Sternberg, 1984; Matthews, 1986; Price, 1986; Klusman, 1993; Thompson, et al., 1994; Schumacher, 1996).

Implications for Exploration Methods/Current Works

The various surface manifestations due to hydrocarbon seepage have led to the development of a number of surface exploration methods, considering geochemistry, geophysics and remote sensing. Soil carbonate methods have to consider the multiple causes for high concentrations of CO_2 in soils, which can result from processes other than microbial oxidation, such as volcanic or geothermal activity, catagenesis or organic matter, micropore filtration, and thermochemical sulfate reduction (Kartsev et al., 1959; Price, 1986; Schumacher, 1996). Even if the CO_2 is a product of hydrocarbon oxidation, the hydrocarbon source could be shallow biogenic methane, rather than thermogenic oil or gas from depth, resulting in no relationship to deep subsurface exploration objectives (Schumacher, 1996). Two of the most used geochemical exploration methods that depend on the presence of soil carbonate are Duchscherer's delta-carbonate method, which measures the amount of CO_2 evolved from the thermal decomposition of soil carbonates at high temperature (Duchscherer, 1981, 1984, 1986; Schumacher, 1996); and Horvitz's "adsorbed" soil hydrocarbon method, which utilizes an acid extraction technique to release hydrocarbons from the fine-grained fraction of the soil sample (Horvitz, 1945; Horvitz, 1985; Schumacher, 1996; Price, 1996). Horvitz's technique is moderately depending on soil calcite concentration, whereas Duchscherer's method is completely dependent on calcite concentration. Horvitz's technique measures the concentration of ethane through pentane in the sample and is therefore specific for thermogenic hydrocarbons, while Duchscherer's method cannot by itself discriminate thermogenic from non-thermogenic calcites (Schumacher, 1996).

The presence of magnetic anomalies over oil and gas fields has been reported for decades, determining that authigenic magnetic minerals can occur in near-surface sediments above petroleum accumulations, and can be detected with aeromagnetic data and confirmed with well cuttings and soils analysis (Schumacher, 1996). However, shallow sedimentary magnetic anomalies are not exclusively associated to petroleum accumulations. There are many examples of false anomalies caused by cultural contamination, geologic structures, and syngenetic magnetic sources (Gay and Hawley, 1991; Gay, 1992). Ellwood and Burkart (1996) documented the fluctuation in oxidizing and reducing conditions, with nonmagnetic phases such as hematite, reducing to magnetite or maghemite, and magnetic phases reverting to nonmagnetic pyrite or siderite under even more highly reducing conditions (Schumacher, 1996).

The electrical tools most appropriated for oil and gas exploration include induced polarization (IP) and magnetotellurics (MT), both of them designed to detect electrochemical altered sediments, i.e. the conductive plume or alteration chimney that may extend from the hydrocarbon

accumulation to the surface (Schumacher, 1996). IP-resistivity method has significant limitations related to the geologic and geochemical conditions required for the formation of the anomalies, which need to be tested with surface geochemistry and shallow drill holes in order to separate anomalies caused by hydrocarbon seepage from false anomalies (Sternberg, 1991; Schumacher, 1996).

The existence of Gamma radiation over oil and gas fields has long been known and forms the basis for radiometric surveys, airborne or ground-based. The major source of soil radioactivity is thought to be Potassium-40, with lesser contributions from Bismuth-214 and Thallium-208. So the radiation over petroleum accumulations have been attributed to precipitation of Uranium salts at the oxidation-reduction boundary at the edge of the inferred hydrocarbon leakage plume, or to the conversion of K-bearing clays and feldspars to kaolinite or other K-deficient clays (Pirson, 1969; Heemstra, et al., 1979; Price, 1986; Saunders, et al., 1993; Schumacher, 1996). There are many factors that can influence the results of these radiation surveys, which have been studied by Weart and Heimberg (1981) and Curry (1984). Heemstra et al. (1979) conducted a study in Kansas and found no correlation between petroleum production and surface radiation, but did find correlation among Gamma radiation and topography, soil type and thickness, bedrock outcrops, and other factors (Schumacher, 1996).

One of the most recent and promissory exploration techniques about mineralogical surface alteration is satellite-based remote sensing. With the development of Landsat systems in 1970s, remote sensing and geographic information systems became a powerful, rapid, and cost-effective tool to acquire images from almost any place on the Earth (Schumacher, 1996; Everett et al., 2002). Major oil companies and many large independents have acquired remote sensing groups, whose work is often a prelude to seismic acquisition; “New technologies in remote sensing and geographic information systems are becoming standard tools for E&P” (Everett et al., 2002). Landsat Thematic Mapper (TM) sensors make it possible to recognize specific mineral compositions, thus becoming a powerful tool in searching for hydrocarbon seepage effects, saving substantial time and money (Everett et al., 2002). Research in the vicinity of Patrick Draw, Lost River, and Lisbon Valley fields during the NASA-Geosat test case project demonstrates that Landsat data can be used to detect hydrocarbon-induced geochemical changes such as the reduction of ferric iron, the conversion of mixed-layer clays and feldspars to kaolinite, and anomalous spectral reflectance of vegetation (Schumacher, 1996). Koyuncu (1992) identified, using Landsat TM data, iron-oxide, carbonate, and hydroxyl-bearing mineral anomalies associated with hydrocarbon-induced alteration and/or uranium mineralization in the San Rafael Swell, Utah; these minerals were then verified by field checks and laboratory analysis.

TM imagery, processed with a powerful spectral analytical algorithm in Yemen, revealed subtle spectral changes in specific units of the Umm er Radhuma Formation, identifying changes in clay and iron content inside and outside the hydrocarbon alteration zone, where there were collected microbial, soil gas and rock samples, and its chemical analysis coincided with 18 of 21 spectral anomalies tested (Everett et al., 2002). Even though drilling confirmed sub-commercial hydrocarbons, the project suggests a strategy for incorporating seeps research into an exploration campaign (Everett et al., 2002).

In marine environments leaking hydrocarbons promote chemosynthetic sea floor communities, produce characteristic bottom topography of crater pits and mounds, and form surface slicks which can be detected by satellite radar. Multispectral (e.g. Landsat) and hyperspectral instruments (e.g. Hyperion and AVIRIS) can distinguish a genuine oil slick from slicks caused by other means like floating vegetation, wind shadows, and downbursts, thus detecting sea-surface hydrocarbons (Everett et al., 2002).

Hyperion is a hyperspectral instrument which collects data in 220 spectral bands, facilitating recognition of a wider variety of mineral species. It can also distinguish a large number of vegetation types, allowing the detection of vegetation effects of hydrocarbon seepage (Everett et al., 2002). Hyperion is called by NASA (2015) the future of remote sensing. AVIRIS is another NASA's hyperspectral instrument which allows precise detection and differentiation of alteration produced by seeping hydrocarbons. AVIRIS data from the Dutton Basin Anticline of central Wyoming's Gas Hills, differentiated between minerals associated with a red bed (Chugwater Formation) and similar iron oxides, sulfides and sulfates associated with seepage (Everett et al., 2002).

Airborne sensors have followed a similar trend. They are growing in sophistication daily, in order to identify hydrocarbon indicators at the surface. In central Mozambique it has been applied to a multi-method airborne geophysical survey with hydrocarbon exploration purposes, including time-domain electromagnetics, magnetometry and Gamma-spectrometry (NGI, 2007). The survey was applied from a rotary and fixed wing aircraft over an area of about 2000 km^2, and its target was measuring near surface resistivity anomalies due to hydrocarbon seepage plumes (NGI, 2007). A seepage alteration zone has been identified since preliminary data interpretation tied to 2D seismic information and regional geology. The anomaly corresponds to a shallow resistive unit which shows high Uranium and low Potassium concentrations (normalized to mean Thorium ratios) (NGI, 2007).

This study focuses on the magnetic and radiometric anomalies produced in soils above Toqui-Toqui and Maná oil fields in Tolima, Colombia, which have accessible public roads, because of their measurable and mappable expression with geophysical field instruments, as a starting point for the selection of soil samples for a mineralogical and elemental analysis through geochemical techniques.

To the authors' knowledge, there are not published reports about this topic in Colombia, so the propose of this research was to search for hydrocarbon indicators evaluating magnetic and radiometric data acquired on Toqui-Toqui and Maná fields, and identify if there are anomalies which can be correlated with their location, as well as identify – by using geochemical techniques – the presence or absence of mineralization in soil samples which lead to explain the geophysical results.

Microbial Effects

Bacteria and other microbes play a profound role in the oxidation of migrating hydrocarbons, and thus are directly or indirectly responsible for the near-surface alteration of hydrocarbons. However, although the role of microorganisms is not always recognized by investigators, there are numerous publications about the influence of microbes in degradation of hydrocarbons (Schumacher, 1996).

Although there are many organisms identified as hydrocarbons oxidizing, bacteria are the most studied (Kartsev et al., 1959; Davis 1952, 1956, 1967; Krumbein, 1983; Atlas, 1984), both aerobic and anaerobic ones (Schumacher, 1996). McKenna and Kallio (1965) also described certain fungi and actinomycetes as hydrocarbons oxidizing in soils (Schumacher, 1996).

Paraffin dirt is one of the byproducts of bacterial oxidation of hydrocarbons. It is a yellow-brownish waxy-appearing soil associated with gas seepages in areas with tropical to temperate climate such as the onshore U.S. Gulf Coast, Colombia, Romania and Burma (Milner, 1925; Davis, 1967; Schumacher, 1996). Davis (1967) created paraffin dirt samples in laboratory, which were indistinguishable from natural ones, by passing

hydrocarbon gas through moist soils to encourage bacterial growth, and defined paraffin dirt as an accumulation of carbohydrates from dead cell walls of fungi and bacteria.

In offshore zones, bacterial mats and suspensions related to oil seepage have been reported from the North Sea, the Santa Barbara Channel, and the Gulf of Mexico (Hovland and Judd, 1988; Sassen, et al., 1993). In the Gulf of Mexico there has been also reported a diverse chemosynthetic community depending on methane and hydrogen sulfide seepage, including mussels, lucinid clams, and tube worms (Kennicutt et al., 1985; Childress et al., 1986; Brooks, et al., 1987; MacDonald et al., 1989, 1990; Reilly et al., 1996; Schumacher, 1996). In marine environments, leaking hydrocarbons also produce characteristic bottom topography of crater pits and mounds, and form surface slicks (Everett, et al., 2002).

There are two metabolic pathways by which microbes consume either free oxygen or chemically bound oxygen in hydrocarbon oxidation. In the first case, aerobic bacteria form carbon dioxide or bicarbonate by the oxidation of hydrocarbon. In the second one, other bacteria reduce sulfate to produce hydrogen sulfide when oxygen is depleted (Schumacher, 1996). These processes can significantly affect the oxidation-reduction potential (Eh) of the environment as well as the pH, leading to new mineral stability fields, and producing minerals through passive grown or as a result of metabolic activity (Schumacher, 1996).

Passive microbial biomineralization include bacterial precipitation of amorphous silica in hot springs and the formation of some authigenic iron oxides, phosphates, carbonates, and clays (Krumbein, 1983; Ferris et al., 1994; Ferris, 1995; Schumacher, 1996). Metabolic activity of microorganisms can result in mineral precipitation by changing the solution chemistry; e.g. an increase in pH can initiate the precipitation of calcium carbonate, and a sulfide production by sulfate-reducing bacteria can lead to the precipitation of some iron sulfides and oxides such as pyrite, greigite, pyrrhotite and maghemite (Reynolds, et al., 1990; Ferris, 1995; Schumacher, 1996). “There are other mineral phases which precipitate directly from bacterial enzyme action, such as the formation of magnetite particles inside the cells of magnetotactic bacteria (Krumbein, 1983; Ferris, 1995)” (Schumacher, 1996).

Hydrocarbon-Induced Diagenetic Alteration

Bacteria are not only responsible for the destruction of hydrocarbons at seep – which can be active, where macro-seeps are ongoing today or have developed from recent tectonic activity, or passive, where concentrations of migrated hydrocarbons are usually low (micro-seeps) (Abrams, 1996) – but they are also responsible for the formation of large volumes of authigenic mineral, including carbonate, elemental sulfur, and iron oxides and sulfides, as well as elements such as uranium (Schumacher, 1996). Models and mechanisms to explain these chemical and mineralogical changes in soils and sediments, due to hydrocarbon accumulations, have been widely proposed and discussed by many authors (Donovan, 1974; Oehler and Sternberg, 1984; Hughes, et al., 1986; Price, 1986; Klusman, 1993; Al-Shaieb, et al., 1994; Thompson, et al., 1994). A simplified summary of the basic reactions and processes is shown in Figure 1 (Schumacher, 1996). This alteration model is intended to provide a general framework within which a wide range of reactions can occur, i.e. it does not represent all possible reactions and processes occurring in near-surface environment.

Hydrocarbons, mainly methane to pentane, migrate upward from the reservoir to the surface through fractures in the lithology by density differentiation (Everett et al., 2002). When they reach near-surface oxidizing conditions, are consumed by aerobic hydrocarbon-oxidizing bacteria, which decrease oxygen in pore waters through the reaction shown in equation 1 (Schumacher, 1996):

1) $$C_nH_{2n+2} + O_{2\,(atmosphere)} \rightarrow CO_2 + H_2O$$

With n= [1, 2, 3, 4, 5] for light hydrocarbons.

These reducing processes develop anaerobic conditions, thus the activity of sulfate-reducing bacteria results in sulfite ion reduction and oxidation of organic carbon to produce reduced sulfur species and bicarbonate ion (Schumacher, 1996). Reduced sulfur species are highly reactive, so they can combine with available iron to form iron sulfides such as Pyrite ($Fe^{2+}S_2$), Marcasite ($Fe^{2+}S_2$), Pyrrhotite ($Fe^{2+}S$) and Greigite ($Fe^{2+}Fe^{3+}{}_2S_4$), and oxides such as Magnetite ($Fe^{2+}O.Fe^{3+}{}_2O_3$) or Maghemite ($Fe^{3+}{}_2O_3$). Finally, as a result of bacterial sulfate reduction, sulfate ion concentration is decreased. Furthermore, bicarbonate is added to pore waters, raising pH and thus promoting precipitation of isotopically light, pore-filling carbonate cements (Schumacher, 1996).

Dissimilatory Metal Reduction

Dissimilatory metal reduction is the process utilized by microbes to conserve energy through the oxidation of organic or inorganic electron donors and reducing oxidized metals from the soils such as Fe^{3+} and U^{6+} (Lovley, 1993). Microbial metal reduction enables organisms to create electrochemical gradients, which provide the chemical energy they require for growth (Lovley, 1993; Glasauer et al., 2003). This reduction process leads to the precipitation of these elements (Fe and U, among others) in a lower oxidation state, which affects their mobility (Schumacher, 1996; Fredrickson et al., 2000; Mohamed Falcón, 2006) and forms new minerals in anomalous concentrations (e.g. not related to the local geology) that can be measured with geophysical field instruments.

In the case of iron, it is reduced from 3+ oxidation state to 2+, allowing the authigenic precipitation of minerals like magnetite (Fredrickson and Gorby, 1996; Zhang, et al., 1997; Dong, et al., 2000; Glasauer, et al., 2003) (equation 2) which produce a magnetic anomalie (Dewangan, et al., 2013).

2) $$Fe^{3+} + e^-_{(bacteria)} \rightarrow Fe^{2+} \qquad (Fe^{2+}(Fe^{3+})_2O^{2-}{}_4)\ \text{Magnetite}$$

Similarly, Uranium reduces from U^{6+} to U^{4+} allowing the precipitation of authigenic uraninite (Meunier et al., 1990; Spirakis, 1996; Schumacher, 1996; Fredrickson et al., 2000) (Equation 3) which can be measure with a scintillation counter because of its significant Gamma radiation.

3) $$U^{6+} + 2e^-_{(bacteria)} \rightarrow U^{4+} \qquad (U^{4+}O^{2-}{}_2)\ \text{Uraninite}$$

Iron Reduction

The presence of magnetic anomalies over oil and gas fields has been examined for decades. A hydrocarbon-induced reduction environment, the same that promotes the formation of uranium, can lead to the precipitation of magnetic iron oxides and sulfides (Schumacher, 1996).

Donovan et al. (1979) reported magnetite in altered Permian rocks overlying Cement Field, Oklahoma, from an aeromagnetic survey and proposed that hydrocarbon migrating from depth caused reduction of hematite to form magnetite, but Reynolds et al. (1984, 1988, 1990) reexamined the occurrence of magnetite at Cement Field by analyzing soil samples and concluded that it represented drilling contamination. However, they documented the presence of ferrimagnetic pyrrhotite and suggested that it precipitated as a result of hydrocarbon seepage. Occurrence of authigenic magnetite has been documented at many hydrocarbon seep sites by Elmore et al. (1987) and McCabe et al. (1987). Sassen et al. (1988, 1989) described the formation of pyrrhotite and other metals in hydrocarbon seep environments at several U.S. Gulf Coast salt domes (Schumacher, 1996). Other studies (Foote, 1987; Foote and Long, 1988; Foote, 1996) have attributed the most of the magnetic anomaly associated with oil and gas fields to the presence of greigite and maghemite in near-surface sediments.

The magnetic mineralization associated with petroleum accumulations, as well as its exploration significance, is controversial, see: Gay and Hawley (1991), Machel and Burton (1991a,b), Gay (1992), Reynolds et al. (1993) and Machel (1996). The hypothesis about magnetic anomalies in near-surface soils generated by hydrocarbon seepage is supported by the general agreement of elevated magnetic susceptibility of soils and sediments with light hydrocarbon soil gas anomalies (Henry, 1988; Saunders et al., 1991; Ellwood and Burkart, 1996; Schumacher, 1996). However, all shallow magnetic anomalies cannot be ascribed to seep-induced alteration; it have to be considered syngenetic magnetic sources such as detrital magnetite, magnetic sedimentary formations, and burned coal seems (Gay, 1992; Schumacher, 1996). Maher and Thompson (1991, 1992) and Liu et al. (1994) reported that increases in soil magnetic susceptibility can response to pedogenic formation of Magnetite and Maghemite, tied to rainfall and climate (Schumacher, 1996).

Fe^{3+} reductions occur often in soils, sediments and the subsurface. The availability of soluble Fe^{3+} is limited in soils, so the predominant form is low-solubility Fe^{3+} hydroxide (Goethite $Fe^{3+}O^{2-}(OH)^{1-}$) and oxide (Hematite $Fe^{3+}{}_2O^{2-}{}_3$) (Hansel and Lentini, 2011; Dewangan et al., 2013). In order to access this insoluble solid-phase of iron, iron-respiring microorganisms utilize soluble electron shuttles and Fe^{3+}-chelating compound, and direct electron transfer via outer membrane enzyme, nanowires, or pili (Coker et al., 2012).

The Fe^{3+}-acquiring mechanism used by the microbes depends on its location, i.e. microbes closer to the mineral surface preferentially use extracellular membrane-bound enzyme to transfer electrons, and microbes that are embedded in between the matrix are more likely to transfer electrons through shuttles or nanowires (Hansel and Lentini, 2011).

Dissimilatory iron-reducing bacteria are fundamental catalysts in iron biogeochemistry because of their ability to couple the oxidation of organic substrates to the reduction of ferric iron (Fredrickson and Gorby, 1996; Zhang et al., 1997; Dong et al., 2000; Glasauer et al., 2003). There is a number of microorganisms with the ability to reduce Fe^{3+}, and it is actually broadly distributed among the known bacterial taxa, but *Geobacter metallireducens* and *Shewanella putrefaciens* were among the first bacteria studied that are able to gain energy for their own growth

by coupling the oxidation of organic matter to the reduction of iron (Fredrickson and Gorby, 1996; Zhang et al., 1997; Dong et al., 2000; Glasauer et al., 2003).

Geobacter metallireducens predominantly uses acetate (a fermentation product) as electron donor (Equation 4) (Lovley, 1993). Fermentation contributes more electrons to Fe3+ during the metabolism than oxygen-based respiration.

4) $$acetate^- + 8Fe^{3+} + 4H_2O \rightarrow 2HCO_3 + 8Fe^{2+} + 9H^+$$

Shewanella putrefaciens, respiring anaerobically, utilizes substrate-level phosphorylation as a primary energy conservation mechanism to sustain growth. Major organic electron donors for this bacterium are formate, lactate and pyruvate, equations 5, 6 and 7, respectively (Lovley, 1993).

5) $$formate^- + 2Fe^{3+} + H_2O \rightarrow HCO_3 + 2Fe^{2+} + 2H^+$$

6) $$lactate^- + 4Fe^{3+} + 2H_2O \rightarrow acetate^- + HCO_3 + 4Fe^{2+} + 5H^+$$

7) $$pyruvate^- + 2Fe^{3+} + 2H_2O \rightarrow acetate^- + HCO_3 + 2Fe^{2+} + 3H^+$$

Lactate and pyruvate are not completely oxidized (they produce acetate), so it is expected for them to have a little contribution in electron flow in Fe^{3+}-reducing environment. Surface contact-mediated electron transfer is significant (Coker et al., 2012).

Fredrickson et al. (1998) concluded that "in sediments where geochemical conditions promote magnetite formation, two-thirds of the ferric iron will be sequestered in a form that may not be available for anaerobic bacterial respiration", so iron-reducing processes are more likely to happen due to aerobic microbes like *Geobacter metallireducens*.

Wilkins et al., (2006), and Hansel and Lentini (2011) described the mechanisms by which Fe^{3+}-reducing bacteria can affect the solubility and mobility of uranium.

Uranium Reduction

The occurrence of uranium has been linked to petroleum by many authors (Eargle and Weeks, 1961; Al-Shaieb, 1977; Goldhaber et al., 1978, 1983; Curiale et al., 1983; Schumacher, 1996). This relation between hydrocarbons and uranium and other heavy metals, such as lead, zinc, and even gold, is due to the reducing environment created by migrating hydrocarbons and associated fluids, which favor the precipitation of uranium and other heavy metals and thereby reduces their mobility (Schumacher, 1996; Fredrickson et al., 2000; Mohamed Falcón, 2006).

Oxidized uranium or uranyl ($[U^{6+}O^{2-}{}_2]^{2+}$) is soluble in groundwater (Kelly, 2010), although when reduced, it precipitates from solution as insoluble uraninite ($U^{4+}O^{2-}{}_2$) (Meunier, et al., 1990; Spirakis, 1996; Schumacher, 1996; Fredrickson et al., 2000).

There are many examples about spatial correspondence of uranium deposits and the geographic limits of subsurface oil and gas accumulations. At Cement Field, Oklahoma, occurs a commercial uranium deposit (Olmstead, 1975; Allen and Thomas, 1984; Schumacher, 1996). Conel and Alley (1985) suggested a genetic relationship among uranium deposits in the Triassic Chinle Formation and the geographic limits of the subsurface oil and gas accumulation in Lisbon Valley Field, Utah. Other authors (Eargle and Weeks, 1961, 1973; Goldhaber et al., 1978, 1983; Reid et al., 1992) related uranium deposits to petroleum accumulations due to reducing environments (Schumacher, 1996).

The action of U^{6+}-reducing organisms results in the transformation of soluble U^{6+} into insoluble U^{4+}. There are two U^{6+}-reducing microorganisms identified: *Geobacter metallireducens* and *Shewanella putrefaciens*, the same ones Fe^{3+}-reducing (Lovley, 1993; Wilkins et al., 2006; Kostka and Green, 2011). The reducing reactions for *Geobacter metallireducens* and *Shewanella putrefaciens* are shown in Equations 8 and 9, respectively (Lovley, 1993).

8) $$acetate^- + 4U^{6+} + 4H_2O \rightarrow 2HCO_3 + 4U^{4+} + 9H^+$$

9) $$H_2 + U^{6+} \rightarrow 2H^+ + U^{4+}$$

The electron donor for U^{6+} reduction for *Shewanella putrefaciens* (Equation 9) is inorganic, differing from the organic electron source used in Fe^{3+} reduction for the same species. The extraction of uranium from the environment is critical because it is an undesirable contaminant, so microbial reduction of U^{6+} represents an efficient option for U^{6+} removal due to the high ratio of pure uranium that can be recovered (Lovley, 1993).

Study Area

Toqui-Toqui and Maná oil fields are in Chicalá Village, Piedras Town, Tolima Department, about 50 kilometers from Ibagué, the capital city of Tolima Department, which is located about 200 kilometers west from Bogotá. Figure 2 shows the location of Piedras Town in Colombia and in Tolima Department, as well as the location of Toqui-Toqui and Maná fields (blue point) (Alcaldía de Piedras-Tolima, 2009).

Location of Toqui-Toqui and Maná fields is on the Magdalena River flood plain on slightly wavy topography, at an elevation of about 320 meters above sea level. It is a warm tropical area with a mean annual temperature around 26°C and mean moisture of about 50% throughout the year. There are two rainy periods in the year alternated by two dry ones (Alcaldía de Piedras-Tolima, 2009).

Geological Framework

Colombia is located on the northwestern corner of South America, a place with a very complex tectonic history which has experienced different geologic events that controlled the distribution, genesis, fill, and bounding structures of its sedimentary basins, which are considered poly-history and varies greatly from basin to basin (Pardo et al., 2007). Colombia can be divided in at least three main tectonic domains explained by Pardo et al. (2007) as follows (Figure 3): (1) The Eastern region, which is bounded to the west by the foothills of the Eastern Cordillera and consists of a Paleozoic and Precambrian basement with a Paleozoic-Cenozoic sedimentary cover that has undergone mild deformation, (2) the Central region comprises the Eastern Cordillera, the Sierra Nevada de Santa Marta, the Magdalena River Valley, and the Central Cordillera extending as far as the Romeral Fault system to the west, and (3) the Western region located at the west of the Romeral Fault system, and composed of Mesozoic-Cenozoic oceanic terranes accreted to the continental margin during Late Cretaceous, Paleogene and Neogene.

Toqui-Toqui and Maná fields are located in the northern section of the Upper Magdalena Valley Basin (Central region). The Upper Magdalena Valley Basin (UMVB) is an intermontane basin located in the upper reaches of the Magdalena River. It is bounded to the north by the Girardot Fold Belt (GFB), to the southeast by the Algeciras-Garzón Fault System (A.G.F.S.), to the northeast by the Bituima-La Salina Fault System (B.S.F.S.), and to the west by Pre-Cretaceous rocks of the Central Cordillera (CC) (Pardo et al., 2007). Figure 4 shows the location of the basin. The Natagaima-El Pata basement high divides the UMVB into two sub-basins: Girardot and Neiva (Butler and Schamel, 1988; Pardo et al., 2007).

The geological map (SGC, 2015) of the study area (Figure 5) shows that in Toqui-Toqui and Maná fields there are outcrops of Honda Formation (n4n6-Sc), Ibagué fan (Q-vc), and Alluvial deposits (Q-al). Honda Formation is a stratigraphic sequence first defined by Hettner (1892), dated by Guerrero (1993) as Neogene age, and whose genesis is continental lacustrine (De Porta, 1966; G. Acosta et al., 2002). It is described as lithic sandstones with greenish-gray claystone insertions and conglomerates (SGC, 2015). Honda Formation is overlying Cretaceous sedimentary rocks on discordant contact (b6k6-Stm), and it is covered in angular unconformity by the Ibagué fan and Quaternary alluvial deposits (Gómez, 2002; SGC, 2015). Ibagué fan is composed by variable thickness volcanoclastic deposits of andesitic composition from Nevado Del Tolima Volcano, mainly pyroclastic flows, lahars and glacial deposits (Gómez, 2002; SGC, 2015). Quaternary alluvial deposits comprise thin unconsolidated current sediments with short extension, which are transported as Torare River's drift material and deposited in floodplains (Cortolima, 1976; Gómez, 2002). Other relevant rock bodies on the map are the Ibagué Batholite (J-Pi), a Jurassic granodiorite intrusive from the Central Cordillera; Triassic metamorphic rocks (T-Mbg3); and the Precambrian basement (MP3NP1-Mag2) (SGC, 2015). Ibagué Fault is a right-lateral strike-slip fault whose length is about 150 km (SGC, 2015).

Petroleum Geology

For the petroleum geology of the UMVB (Figure 3) the reader should refer to Barrero et al. (2007), who describes it as a Neogene foreland basin bounded to the east and to the west by Precambrian to Jurassic basement uplifts (i.e. the flanks of the Eastern and Central Cordillera, respectively), which contains a Cretaceous continental to transgressive sequence overlaid by one of the most important reservoir sandstone units (Caballos Fm.), followed by an Albanian to Campanian sequence of limestones, shales and cherts, which contain the organic rich source rocks, and are overlaid by a Campanian to Maastrichtian sandstone unit (Monserrate Fm.) which is also an important reservoir rock of the

basin. The Cenozoic sequence, deposited during the collisional events that shaped the current Colombian sedimentary basins, have Paleogene and Neogene non-marine sediments.

The UMVB, with an area extend of about 26,200 km^2 (i.e. 6,474,000 acres), has 631 MBO discovered oil reserves and 123 GCF discovered gas reserves, with 210 wildcat wells and 36 discovered fields, and by 2007 was producing 18 million barrels of oil per year from 28 fields (Barrero et al., 2007).

Santacruz (2014) mentions as source rock for both Toqui-Toqui and Maná fields the shales and limestones of Villeta Group, which is correlated with La Luna, Bambucá and Tetúan formations, and whose high organic content is attributed to two worldwide anoxic events of Middle Albanian and Turonian age. The predominant kerogen in these source units is type II, they contain on average 1%-4% of T.O.C., and Hydrogen index varies between 100-650 mgHc/gc (Barrero et al., 2007). Barrero et al. (2007) define the migration as a continuous process that started soon after the first contractional event of Late Cretaceous age through today, with remigration to present day traps starting during Miocene, after deposition of thick molassic deposits. Reservoir rocks of Toqui-Toqui and Maná fields are Doima, Chicoral and Monserrate formations, with Guaduala, Potrerillo and Barzalosa formations as seal rocks, respectively (Santacruz, 2014).

UMVB is a complex basin characterized by multiple deformation and alternated periods of subsidence and erosion since Maastrichtian to the present (Barrero et al., 2007). According to Santacruz (2014), the area of Toqui-Toqui and Maná fields is associated with a structural high, which was originated from the oblique convergence of the Ibagué Fault and Alvarado Fault (also known as Cambao Fault) against Ibagué batholite. The structure of Maná Field has a geometric design corresponding to a monocline dipping to the east, which sinks in direction west-east at basement level due to a normal fault, underneath the thrust fault system (which include Bituima and Cambao faults) associated with the west flank of the East Cordillera. The structure of Toqui-Toqui Field is a simple monoclonal dipping to the northeast, with a variable slope ranging between 11° and 14°, which encloses an area of 2040 ac and is bounded by compressional structures, some of which have slip components (Santacruz, 2014).

During 1980's and 1990's decades the basin was actively explored for hydrocarbon, but it is believed that important oil reserves remain trapped in stratigraphic and sub-thrust plays, which would add new reserves by the development of new and unconventional play concepts (Barrero et al., 2007). According to well information available (ANH, 2014), it is known that the greatest true vertical depth is about 6000 feet. The mean daily production of Toqui-Toqui and Maná fields is 568 and 1387 BOPD, respectively (Santacruz, 2014).

Soils

According to the general soils study of the Tolima Department (IGAC, 2004), on the area of Toqui-Toqui and Maná fields there are three soil units: MWA Unit, MWI Unit, and LWA Unit. They are shallow and low-productive soils exposed to strong erosion, with low organic matter content, and with the presence of A, B and C horizons, where can be found metallic oxides and hydroxides, clay materials, some roots, and influence from the outcrop lithology.

The Unit MWA has the association Lithic Ustorthents (LU)-Typic Ustorthents (TU), 50% LU, 30% TU, and 20% of outcrop rock inclusions (IGAC, 2004). The soils of this unit are shallow to intermediate-deep, few evolved, highly drained, and have low content of organic matter. They are in elevations between 400 and 900 meters above sea level, in sloped and steep reliefs. These soils develop above sedimentary materials, mainly sandstones and claystones, and are affected by laminar hydric erosion in moderate to severe grade.

The Unit MWI has the association Typic Ustropepts (TUp)-Lithic Ustorthents (LU), 60% TUp, 10% LU, and 10% of outcrop rock inclusions (IGAC, 2004). These soils are in wavy to rough hills with slopes of about 25-50%. They present moderate to severe erosion, and are very shallow and moderate-deep, with a good to excessive drain. Their parental materials are claystones, sandstones, conglomerates and limestone inclusions, and have low content of organic matter.

Unit LWA has the association Lithic Ustorthents (LU) - Typic Ustorthents (TU), 40% LU, 35% TU, and 25% of outcrop rock inclusions (IGAC, 2004). The soils of this unit are shallow with moderate and severe erosion, and are present in wavy to steep relieves with slopes ranging from 7% to 75%. They are developed from sandstones, tuffs and claystones.

Methodology

Field Work

The field work was carried out on October 11 and 12, 2014, where magnetic and radiometric data were taken, as well as soil samples from Toqui-Toqui and Maná fields and surrounding areas, for geophysical and geochemical analysis, respectively. Acquisition points are uniformly distributed on the public access roads to the wells. A summary of the data and soil samples collected in the field is shown in Table 1.

Geophysical Analysis

The processing of the magnetic data was done based on the procedure described by Cárdenas Contreras and Castillo López (2013) by using the Analytic Signal technique.

The Analytic Signal (AS) is an interpretation technique for magnetic and gravimetric data. It was defined by the first time by Ville (1948), and its 2D and 3D results have been shown to give precise information about the location, shape and depth of magnetic anomaly sources, thus leading to a geological imaging including faults and lithologic contacts, even in low magnetic latitude areas like Toqui-Toqui and Maná fields (Nabighian, 1972, 1974, 1984; MacLeod et al., 1993; Phillips, 2000; Cárdenas Contreras and Castillo López, 2013). For geological models, the Analytic Signal is a symmetric positive function located above the body where the anomaly is generated, and its amplitude is only dependent on the depth by the relation shown in equation 10 (Phillips, 2000; Keating and Sailhac, 2004; Cárdenas Contreras and Castillo López, 2013).

10) $$x = \sqrt{2}h$$

Where x is the horizontal extension of an anomaly on the Analytic Signal and h is the depth to the source of the anomaly.

The First Vertical Derivative (FVD) and the Second Vertical Derivative (SVD) of the magnetic field allow the identification of geological sources for the anomalies at surface and near surface, respectively, as well as the anomalous edges. Vertical derivatives technique, which amplifies the more the high frequencies when the major the derivative grade is, has been a standard processing method for highlighting the high frequency values from the whole data by analyzing up to second order derivatives, because for major derivative grades there is too much noise (i.e. noise is also amplified) (Nabighian, 1984; Cárdenas Contreras and Castillo López, 2013).

The 3D Analytic Signal (AS) of the Magnetic Field Strength was calculated, as well as its first and second vertical derivatives. With this information, contour maps were made and analyzed in relation with radiometric, geological, and productive-wells data.

For the interpretation of the Gamma-Ray data, contour maps were made and analyzed in relation with magnetometric, geological, and productive-wells data. All the contour maps were done by using minimum curvature gridding with a grid cell size of 250 m, which is the average distance between sampling points.

Geochemical Analysis

Mineralogical and elemental analyses were made to 10 selected soil samples, which were chosen based on Gamma-Ray (GR) values from the field, thus considering the 5 samples from the points with the highest GR values and the 5 samples from the points with the lowest ones.

For the mineral identification, the X-Ray diffraction (XRD) technique was used. After applying XRD to the 10 selected samples it was necessary to make a magnetic separation for each of them, because of the complex mineralogical composition which led to overlapping of peaks from different minerals, thus getting 20 samples. This process allowed the calculation of clays, magnetic and non-magnetic minerals proportions for each sample. After the analysis of the 20 samples, the one with the highest proportion of magnetic minerals was concentrated by density differentiation to remove undesired mineral responses from the diffractograms.

The chemical composition analysis was done by using Major Elements Fusion ICP (FUS-ICP) and Trace Elements Fusion ICP/MS (ICP-MS).

Results and Discussion

Analytic Signal

The Analytic Signal of the Magnetic Field Strength and its 3D visualization are shown in Figure 6. There are two anomalous sources clearly identified, which are disrupted in the middle. The depth of the sources is estimated by symmetry criteria of the Gaussian bells representing their location. The horizontal yellow line on the 2D map in Figure 6 represents 1426 m, which led to a half depth of 1008 m, thus leading to a total depth of 2016 m. For the anomalous peak on the left, this line represents 2860 m, which led to 2022 m depth.

The disruption between the two Gaussian bells is associated with a thrust fault, since both peaks in the map are aligned but the one on the left has higher values of the Analytic Signal, which implies more depth, so being related with the footwall of the disruption between the two Gaussian bells is associated with a thrust fault, since both peaks in the map are aligned but the one on the left has higher values of the Analytic Signal, which implies more depth, so being related with the footwall of the fault. The model of the Girardot Sub-Basin (where Toqui-Toqui and Maná fields are) proposed by Montes (2001) (Figure 7) matches with the analysis from Analytic Signal in the estimated depths to the basement and in the orientation of Cambao Fault. According to the geological map of the area (SGC, 2015), Cambao Fault is covered and its location is not precisely known. However, the description of the petroleum geology of Toqui-Toqui and Maná oil fields mentions the convergence of Cambao Fault and Ibagué Fault towards Ibagué batholite as the cause of the monocline which represents the structural trap for the fields (Santacruz, 2014).

Vertical Derivatives of the Magnetic Field Strength

Analysis of the Analytic Signal technique allows the identification of sources of magnetic anomalies related to geological features and structures at mappable scale. For the identification of the sources of near-surface anomalies, it is necessary to use the vertical derivatives of the Magnetic Field Strength. The first vertical derivative of the Magnetic Field Strength allows the identification of anomalous sources at surface, and the second vertical derivative, which amplifies more the high frequencies, led to the location of near-surface anomalies' sources and anomalous edges in the local geology.

The First and Second Vertical Derivatives of the Magnetic Field Strength (Figure 8) show an isolated high value inside the area of Toqui-Toqui and Maná oil fields, which cannot be explained by the local geology since the distribution of the volcanoclastic sediments from Nevado Del Tolima Volcano is not isolated. So this peak can be associated with the location of the source of a magnetic anomaly related to light hydrocarbons migration to the surface, generating reducing conditions, and thus leading to the authigenic formation of magnetite.

Magnetic Field Strength and Gamma-Radiation

Figure 9 shows maps of the Magnetic Field Strength and GR for comparison, where the coincidences and differences are pointed out with orange arrows and blue arrows, respectively. Black lines represent SW-NE profiles for Magnetic Field Strength and GR, which are shown in Figure 10 and Figure 11, respectively.

It can be observed from Figure 9 that the highest values of GR are located on the SW edges of the area of Toqui-Toqui and Mana fields, while there is a notable distribution of low values inside it. This is basically the opposite distribution of the magnetic response, which highest values are inside the area of Toqui-Toqui and Maná oil fields and are surrounded by low values, which can suggest a relation with the spatial distribution of the hydrocarbons.

There is no relation of these responses with the local geology (Figure 12), since both GR and Magnetic Field Strength vary from the lowest values to the highest ones in the same lithological bodies. From Figure 9, Figure 10, and Figure 11 it can be observed that both measurements have high values at the western border of the fields, and that the maximum values of the Magnetic Field Strength coincide with the minimum

ones of GR inside the area of Toqui-Toqui and Maná. The relationship between Gamma-Radiation and Magnetic Field Strength can be summarized in the analysis of the profiles in Figure 10 and Figure 11.

The maximum values of the Magnetic Field Strength can be easily related to the oil fields (i.e. to the migration of light hydrocarbons to the surface) because of the spatial correspondence between them, considering the location of the anomaly source given by the vertical derivatives. This can be explained as the reduction of Fe^{3+} from Hematite and Goethite in soils due to the reducing conditions produced by the hydrocarbon leak age, which led to the formation of authigenic Magnetite, thus producing the magnetic anomaly. This effect can be seen as the Gaussian relation proposed by Schumacher (1996) in his generalized model of hydrocarbon-induced geochemical and geophysical alteration of soils and sediments (Figure 1).

The high GR measurements at the western border of the oil field, and its decreasing value to the east can be seen as the aureole effect, also described by Schumacher (1996) in his model for hydrocarbon-induced alteration of soils (Figure 12), allowing the reduction process to be possible only at the limit between oxidizing and reducing areas.

U^{6+} can be reduced under the same conditions of Fe^{3+} but, since it is soluble, it is drained from soils by surface and ground water, so it precipitates as soon as it finds a reducing environment on its way to lower lands. Toqui-Toqui and Maná oil fields are located on the way of the drainages that flow eastward from the Central Cordillera towards the Magdalena River, so that can be the reason why the maximum values of Gamma-Radiation are at the western border of Toqui-Toqui and Maná oil fields (i.e. U^{6+} is precipitated as U^{4+} before water flows can cross over the area of Toqui-Toqui and Maná fields). This does not only explain the location of the maximum values of GR measurements, but also its considerable decrease eastward.

These reducing processes are mediated by bacteria, which find it easier to reduce soluble U^{6+} than mineralized Fe^{3+}, which explains why there are low Magnetic Field Strength values where there are the maximums of GR (i.e. to the left of the western border of the fields). On the other hand, after passing by the western border of the oil fields, the U^{6+} content decreases significantly, which allows the precipitation of Fe^{2+} from the reduction of the abundant Fe^{3+}. This is seen as low GR values in the locations where the Magnetic Field Strength is highest, inside the area of Toqui-Toqui and Maná oil fields. Figure 13 shows a schematic model of this explanation.

Chemical Composition

Because of the significant influence of volcanism from the Central Cordillera in the study area, it was necessary to identify the parental material of the soils in order to distinguish it from authigenic minerals. The chemical analysis focused on the determination of the parental material of the soils and the identification of alteration features by comparison with the results of Jaramillo (1980) for the lavas of the Nevado Del Ruiz Volcano, which is genetically related to Nevado Del Tolima Volcano (and next to it) in the Central Cordillera.

FUS-ICP results are shown in Table 2. According to TAS classification, the soil samples have dacitic and andesitic composition (Figure 14), and they are all sub-alkaline (Figure 15). These results coincide with the ones exposed by Jaramillo (1980), who used the Miyashiro (1974) classification for Sub-Alkaline rocks to define the ones he studied as part of a volcanic rock series that exhibit a relative large variation in SiO_2

while the FeO(T)/MgO ratio is almost constant or show only small increases (i.e. Calcalkaline). This is the same behavior shown by the soil samples used for this study (Figure 16), which confirms the significant presence of intermediate volcanic material in the surface of Toqui-Toqui and Mana oil fields and the surrounding areas.

These results show the same classification for all the samples, which does not correspond to the geology of the sampled points (Figure 17), located in different lithological bodies. Harker (1909) diagrams (Figure 18) show the typical response of elemental oxides for volcanic rocks, except for K_2O, which decreases when total silica content (i.e. SiO_2) increases.

Figure 19 shows the elements producing magnetic and radiometric anomalies (i.e. Fe, U, Th and K) with respect to the total silica content (i.e. SiO_2). It can be observed that all the elements have high (Fe, Th and U) to medium (K) negative correlation with the silica content.

The results for Gamma-radiating elements does not correspond with the general response of a volcanic rock, where they have positive correlation with SiO_2, which suggests a diagenetic source of Gamma-Radiation. It can be observed from the Harker diagram for Fe (Figure 18) that for the soil samples studied the Fe content decreases at a lower rate than it does in the reference volcanic samples, which suggests a diagenetic source of magnetic minerals. This anomalous contents of Gamma-radiating elements and Fe suggest an alteration in the original composition of the soils (i.e. its parental material) related to the reducing conditions due to the migration of light hydrocarbons to the surface.

Figure 20 shows the positive correlation existing between Gamma-radiating elements and the GR measurements from the field. U and Th show the highest correlation. This also can be observed from Figure 21, where it is shown the high positive correlation between U and Th, while it is medium positive between U and K. This suggest that the radiometric anomaly is more influenced by Th and U content than by K content.

Figure 22 shows the high positive correlation existing between U and Fe, which does not exist in volcanic rocks under normal conditions (i.e. it would be negative), thus supporting the idea of the alteration of the soils. Figure 23 shows REE (Rare Earth Elements) diagram (normalized chondrite) (McDonough and Sun, 1995), which is compared with the andesite FM-4 studied by Jaramillo (1980). Soil samples have the typical response of intermediate volcanic rocks.

The chemical composition analysis of the soil samples shows that they have intermediate volcanic parental material since major elements analysis and REE have the same response than the samples studied by Jaramillo (1980). However, there are anomalous behaviors in Gamma-radiating elements and Fe which suggest an alteration due to diagenetic processes. This is analyzed with the mineral identification through XRD.

Mineral Composition

Magnetites as a product of the activity of the volcanoes from the Central Cordillera have a significant proportion of Titanium and Iron oxides with a wide range of compositional variations (Jaramillo, 1980), so it is expected to find two species of Magnetite: Titanium-Magnetite and stoichiometric Magnetite (i.e. from authigenic precipitation). Twenty minerals were identified (listed in Table 3). They are sorted vertically by

decreasing average abundance in all the soil samples, which are sorted horizontally by increasing GR value. The ratios of clay minerals, non-magnetic minerals, and magnetic minerals for the samples are plotted in Figure 24.

The minerals found in the samples correspond to the typical association of andesitic rocks: intermediate composition Plagioclase (i.e. Andesine in nine samples and Labradorite in one), two Pyroxenes (i.e. mainly Ferroan Enstatite, and Augite in less proportion), two Amphiboles (i.e. Riebeckite and Pargasitic Hornblende), Biotite and its alteration products (i.e. Chlorite and Vermiculite), Zircon, Apatite, and Fe-Ti oxides/hydroxides (i.e. Magnetite, Ilmenite, Goethite, Hematite and Rutile). This mineral association coincides with the results obtained by Jaramillo (1980) in his petrographic and geochemical analysis of rocks from Nevado del Ruiz Volcano, which is located in the Middle Cordillera and has the same petrogenesis of Nevado Del Tolima Volcano, whose deposits are transported by the Ibagué fan to the area next to the Toqui-Toqui and Mana fields (SGC, 2015). The Quartz proportion does not correspond directly with the expected for andesitic composition because an important part of the samples correspond to clay minerals (39.9% in average).

The volcanic parental material of the samples represents a challenge for the correct identification of magnetic anomalies due to authigenic Magnetite. However, Magnetite from andesitic rocks has significant amounts of Titanium (Jaramillo, 1980), which allows the distinction between two Magnetite species: Titanian Magnetite and stoichiometric Magnetite (i.e. authigenic), both of which were identified by XRD.

There were also identified Fe-bearing Carbonates in the soil samples (i.e. Ferroan-Dolomite and Siderite), which can be related to surface manifestations of hydrocarbon seepage (Schumacher, 1996) since they do not correspond to the volcanic parental material or to the local geology (SGC, 2015). From Figure 24 it is observed that the magnetic proportion in the samples increases with GR and the non-magnetic and clay minerals ratios are very variable over the samples, which predicts an important variability in the composition and genesis of the soils.

Table 4 shows the mineral association found in the samples, classified by mineral species. They are, in decreasing average abundant order, Pyroxene (Ferroan Enstatite + Augite), Quartz, Plagioclase (Andesine/Labradorite), Amphibole (Riebeckite + Pargasitic Hornblende), Biotite (Biotite + Chlorite + Vermiculite), Zircon, Fe-Ti Oxides/Hydroxides (Magnetite + Ilmenite + Goethite + Hematite + Rutile), Carbonate (Ferroan-Dolomite + Siderite), and Apatite.

Figure 25 shows plots of Biotite, Zircon, Apatite and Amphibole vs. GR in order to identify the correlation between these Gamma-radiating minerals and the GR measurements in the field. It can be observed that the correlation of Biotite, Zircon and Amphibole with GR is null, while the correlation between Apatite and GR is medium. However, this result is not enough for explaining the GR values and the anomaly shown in the geophysical analysis, thus it is proposed to exist Uraninite in proportion less than the detection limit for XRD technique (~2%), which was predicted from geophysical and chemical composition results.

Figure 26 shows the very high positive correlation existing between Fe^{2+} and Fe^{3+} minerals (i.e. correlation coefficient R2=0.93). Fe^{3+} is reduced to Fe^{2+} (i.e. in reducing environments as the one generated at surface above hydrocarbon accumulations) from Hematite ($Fe^{3+}{}_2O^{2-}{}_3$) and Goethite ($Fe^{3+}O^{2-}(OH)^{1-}$), allowing the formation of Magnetite ($Fe^{2+}O^{2-}.Fe^{3+}2O^{2-}{}_3$), Siderite ($Fe^{2+}C^{4+}O^{2-}{}_3$), Ilmenite ($Fe^{2+}Ti^{4+}O^{2-}{}_3$), and Ferroan-Dolomite ($Ca(Mg, Fe)(CO_3)_2$). These minerals do not correspond to the genesis of the soils and their presence in the samples is explained by this authigenic process.

It is important to highlight from Figure 26 that for Fe^{3+} values less than 3% the ratio Fe^{2+}/Fe^{3+} (i.e. 0.27) is less than the one for Fe^{3+} values bigger than 3% (i.e. 0.44); so 3% can be interpreted as an inflection point for Fe^{3+} reduction.

Figure 27 shows the diffractogram of the sample P128-P-C, which was concentrated by gravitational differentiation by the use of tray and dense liquids (i.e. methylene iodide). There can be clearly distinguished Titanian-Magnetite (red) and stoichiometric Magnetite (blue) in the zoom-in window; each one represents 0.2% of the whole sample.

From XRD analysis it can be observed that all the soil samples have a mineral association corresponding to andesitic rocks as parental material. However, there are significant differences in the relative mineral composition abundances for each sample, which are located in a relatively short area, thus suggesting strong spatial variability in the parental material. From this, and considering the geological setting, it can be inferred that the soils were developed over volcanic materials transported (i.e. not in-situ) by alluvial flows and mixed with local depositions of volcanic ash, whose volcanic glass can explain the variable and significant proportion of clay minerals, as a product of its alteration. This led to a mechanical separation of the materials from which the soils were formed in the sedimentation process. Figure 28 shows a cross-cutting section from the location of one of the sampled points that shows different sedimentation events before the formation of the soil.

The variable composition in the mixing from which the soils of the studied area were developed led to a very complex data (i.e. geophysical and mineralogical) with significant noise that obstructs the identification of diagenetic processes affected by reducing conditions related to Toqui-Toqui and Maná oil fields. However, there have been identified minerals (i.e. stoichiometric Magnetite, Ferroan-Dolomite and Siderite) that do not correspond with the local geology nor with volcanic soils, and can be predicted from dissimilatory metal reduction to be related to the migration of hydrocarbons to the surface.

There have not been identified minerals that correlate significantly with GR measurements, so it is propose the existence of authigenic Uraninite, which is predicted from geophysical and chemical composition analyses, in proportions less than the detection limit of XRD.

Conclusions

The migration of light hydrocarbons (C1-C5) to the surface produces anaerobic conditions that force aerobic bacteria to use dissimilatory metal reduction to conserve energy, thus oxidizing organic or inorganic electron donors and reducing oxidized metals from the soils such as Fe^{3+} and U^{6+}. This reduction process leads to the precipitation of these elements (Fe and U, among others) into a lower oxidation state, which affects their mobility and forms new minerals in anomalous concentrations (e.g. not related to the local geology) that can be measured with geophysical field instruments.

Petroleum exploration begins with the search for hydrocarbon indicators at the surface. With the appropriate geological information and geophysical data, mineralogical changes can be identified, induced in soils by the presence of hydrocarbons and its migration to the surface.

Magnetic and Radiometric signatures correlate spatially with Toqui-Toqui and Maná oil fields. The magnetic signature shows a Gaussian effect inside the area of the oil fields due to the precipitation of Fe2+ on the zone indicated by the vertical derivatives of the Magnetic Field Strength

to be the location of the source of the surface anomaly. The radiometric signature shows an aureole effect on the western border of the oil fields due to the precipitation of U4+. The precipitation of Fe2+ and U4+ is related to diagenetic processes associated to reducing conditions due to hydrocarbons migration to the surface. The difference in their location is due to the mobility of soluble U6+, which precipitates as soon as it gets to the border of the reducing zone, thus deflecting on its eastward way to the Magdalena River and leading to the reduction of the mineralized Fe3+ above the area of Toqui-Toqui and Maná oil fields, which produces the magnetic anomaly correlated to such zone.

The Analytic Signal technique is a powerful tool in the exploration of the subsurface that can be combined with near-surface geophysical data for hydrocarbon exploration purposes. Its analysis was combined with information about the petroleum geology of Toqui-toqui and Maná oil fields and regional geology, allowing the identification of important structural features.

The chemical composition analysis of the soil samples shows that they have intermediate volcanic parental material, since major elements analysis and REE have the same response as the samples from Nevado Del Ruiz Volcano studied by Jaramillo (1980). However, Gamma-radiating elements and Fe exhibit alteration, which suggests low grade diagenesis.

The mineral association of the soil samples studied corresponds to andesitic rocks as parental material, which is typical of the Central Cordillera in the northern Andes. This produces masking on the geophysical signatures measured and represents an obstacle on the identification of minerals attributed to diagenetic processes related to the migration of hydrocarbons to the surface. However, evidence of the presence of minerals not related to the parental material nor to the local geology (i.e. stoichiometric Magnetite, Ferroan-Dolomite and Siderite) was found. Their authigenic formation can be predicted from dissimilatory metal reduction associated with the migration of hydrocarbons to the surface on Toqui-Toqui and Maná oil fields.

There have not been identified minerals that correlate significantly with GR measurements, so it is proposed the existence of authigenic Uraninite, which is predicted from geophysical and chemical composition analyses, in proportions less than the detection limit of XRD. A significant variability was found in the mineral proportion of the soil samples studied. This is explained by mechanical differentiation during sedimentary processes, which is attributed to different events of alluvial transport of volcanoclastic material from the Central Cordillera and volcanic ash fall. The alteration of the volcanic glass led to the high and variable proportion of clay minerals in the soil samples.

The composition of soils as well as the geophysical anomalies do not correspond with the lithology described by SGC (2015) for this area. This is due to the fact that the geological map made by SGC (2015) represents a description of the bedrocks and does not necessarily describe the outcrops, which are the transported parental materials of the soils used for this study. The geophysical anomalies are attributed to the authigenic formation of Magnetite and Uraninite due to the migration to the surface of light hydrocarbons.

Acknowledgements

The authors would like to especially recognize the cooperation of Gmas Laboratory in providing the support and sponsorship during the development of this project, as well as Universidad de los Andes and Colombian Association of Petroleum Geologists and Geophysicists (ACGGP) for their assistance regarding to the development of this artice.

Selected References

Abrams, M.A., 1996, Distribution of subsurface hydrocarbon seepage in near-surface marine sediments, *in* D. Schumacher and M. A. Abrams, eds., Hydrocarbon migration and its near-surface expression: AAPG Memoir 66, p. 1-14.

Acosta, G., R. Guatame, A. Caicedo, and J.I. Cárdenas, 2002, Grupo Honda (Ngh), *in* Mapa Geológico de Colombia, Plancha 245 Girardot. Escala 1:100.000, Memoria Explicativa, Bogotá: INGEOMINAS, p. 51-53.

Alcaldía de Piedras-Tolima, 2009, Piedras-Tolima. Website accessed March 16, 2017. http://www.piedras-tolima.gov.co/mapas_municipio.shtml

Allen, R.F., and R.G. Thomas, 1984, The uranium potential of diagenetically altered sandstone of the Permian Rush Springs Formation, Cement district, southwest Oklahoma: Economic Geology, v. 79, p. 284-296.

Al-Shaieb, Z., 1977, Uranium potential of Permian and Pennsylvanian sandstones in Oklahoma: AAPG Bulletin, v. 61, p. 360-375.

Al-Shaieb, Z., J. Cairns, and J. Puckette, 1994, Hydrocarbon-induced diagenetic aureoles: Indicators of deeper leaky reservoirs: Association of Petroleum Geochemical Explorationists Bulletin, v. 10, p. 24-48.

ANH, 2014, Agencia Nacional de Hidrocarburos. Website accessed March 16, 2017. http://www.anh.gov.co/Asignacion-de-areas/Paginas/Mapa-de-tierras.aspx

Atlas, R.M., 1984, Petroleum Microbiology, New York, Macmillan Company, 692 p.

Barrero, D., J.F. Martínez, C.A. Vargas, and A. Pardo, 2007, Petroleum Geology of Colombian Basins, *in* ANH & B. & M. Exploration Ltda, eds., Colombian Sedimentary Basins: Nomenclature, Boundaries and Petroleum Geology, A New Proposal, Bogotá: Agencia Nacional de Hidrocarburos Colombia, p. 84-86.

Brooks, J.M. et al., 1987, Deep-sea hydrocarbon communities: evidence for energy and nutritional source: Science, v. 238, p. 1138-1142.

Butler, K., and S. Schamel, 1988, Structure along the eastern margin of the central Cordillera, upper Magdalena Valley, Colombia: Journal of South America Earth Science, v. 1, p. 109-120.

Cárdenas Contreras, A., and L.A. Castillo López, 2013, Interpretación de datos gravimétricos con la Señal Analítica 3D. Estudio de caso: Los Naranjos-Facatativá (Colombia), Boletín de Geología, UIS, v. 35/1, p. 97-107.

Cárdenas Contreras, A., H.J. Fuentes, Castillo L.A. López, and J.C. Acosta Chady, 2014, Geomagnetismo, *in* Fundamentos teóricos y su aplicación en los métodos de potencial geomagnético y gravimétrico, Bogotá: Universidad Distrital Francisco José de Caldas, p. 15-33.

Childress, J.J. et al., 1986, A methanotrophic molluscan (Bivalvia, Mytilidea) symbiosis: mussels fueled by gas: Science, v. 233, p. 1306-1308.

Coker, V.S. et al., 2012, Characterization of the dissimilatory reduction of Fe(III)-oxyhydroxide at the microbe–mineral interface: the application of STXM–XMCD: Geobiology, v. 10, p. 347-354.

Conel, J. E., and R.E., Alley, 1985, Lisbon Valley, Utah uranium test site report, *in* M. J. Abrams, J.E. Conel, H.R. Lang, and H.N. Paley, eds., The Joint NASA/Geosat Test Case Project, final report: AAPG Special Publication, pt. 2, p. 8-1, 8-158.

Curiale, J.A., S. Bloch, J. Rafalska-Bloch, and W.E. Harrison, 1983, Petroleum-related origin for uraniferous organic-rich nodules of southeastern Oklahoma: AAPG Bulletin, v. 67, p. 588-608.

Curry, W.H., 1984, Evaluation of surface gamma radiation surveys for petroleum exploration in the deep Powder River basin, Wyoming, *in* M.J. Davidson and B. M. Gottlieb, eds., Unconventional methods in exploration for petroleum and natural gas, III., Dallas, Texas: Southern Methodist University Press, p. 25-39.

Dalziel, M.C., and T.J. Donovan, 1980, Biogeochemical evidence for subsurface hydrocarbon occurrence, Recluse oil field, Wyoming: preliminary results: USGS Circular, v. 837, p. 11.

Davis, J.B., 1952, Studies on soil samples from a "paraffin dirt" bed: AAPG Bulletin, v. 36, p. 2186-2188.

Davis, J.B., 1956, Microbial decomposition of hydrocarbons. Industrial and Engineering Chemistry, v. 48/9, p. 1444-1448.

Davis, J.B., 1967, Petroleum Microbiology, New York: Elsevier, p. 604.

De Porta, J., 1966, Geología del extremo sur del Valle Medio del Magdalena entre Honda y Guataquí: UIS Boletín Geológico, v. 1347, p. 22-23.

Dewangan, P. et al., 2013, Diagenesis of magnetic minerals in a gas hydrate/cold seep environment off the Krishna–Godavari basin, Bay of Bengal: Marine Geology, v. 340, p. 57-70.

Dong, H. et al., 2000, Mineral transformation associated with the microbial reduction of magnetite: Chemical Geology, v. 169, p. 299-318.

Donovan, T.J., 1974, Petroleum microseepage at Cement, Oklahoma--evidence and mechanisms: AAPG Bulletin, v. 58, p. 429-446.

Donovan, T.J., R.J. Forgey, and A.A. Roberts, 1979, Aeromagnetic detection of diagenetic magnetite over oil field: AAPG Bulletin, v. 63, p. 245-248.

Duchscherer, W., 1981, Carbonates and isotope ratios from surface rocks, a geochemical guide to underlying petroleum accumulations, *in* B. M. Gottlieb, ed., Unconventional methods in exploration for petroleum and natural gas, symposium II. Dallas, Texas: Southern Methodist University Press, p. 201-218.

Duchscherer, W., 1984, Geochemical hydrocarbon prospecting, with case histories: PennWell Publishing, Tulsa, Oklahoma, p. 196.

Duchscherer, W., 1986, Delta carbonate hydrocarbon prospecting. In: M. J. Davidson, ed. Unconventional methods in exploration for petroleum and natural gas, symposium IV. Dallas, Texas: Southern Methodist University Press, p. 173-182.

Eargle, D.H., and A.M.D. Weeks, 1961, Possible relationship between hydrogen sulfide-bearing hydrocarbons in fault line oil fields and uranium deposits in the southeast Texas coastal plain: USGS Professional Paper, v. 424-D, p. D7-D9.

Eargle, D.H., and A.M.D. Weeks, 1973, Geologic relations among uranium deposits, south Texas coastal plain region, U.S.A., *in* G.C. Amstutz and A.J. Bernard, eds., Ores in Sediments, Springer-Verlag, New York, p. 101-113.

Ellwood, B.B., and B. Burkart, 1996, Test of Hydrocarbon-Induced Magnetic Patterns in Soils: The Sanitary Landfill as Laboratory, *in* D. Schumacher and M.A. Abrams, eds., Hydrocarbon migration and its near-surface expression: AAPG Memoir 66, p. 91-97.

Elmore, R.D. et al., 1987, Evidence for a relationship between hydrocarbons and authigenic magnetite: Nature, v. 325, p. 428-430.

Everett, J.R., R.J. Staskowski, and C. Jengo, 2002, Remote sensing and GIS enable future exploration success: World Oil, v. 223/11.

Feely, R.W., and J.L. Kulp, 1957, Origin of Gulf Coast salt dome sulfur deposits: AAPG Bulletin, v. 41, p. 1802-1853.

Ferris, G.F., 1995, Microbes to minerals: Geotimes, v. 409, p. 19-22.

Ferris, G.F., R.G. Wiese, and W.S. Fyfe, 1994, Precipitation of carbonate minerals by microorganisms: implications for silicate weathering and the global carbon dioxide budget: Geomicrobiology Journal, v. 12, p. 1-13.

Foote, R. S., 1987, Correlations of borehole rock magnetic properties with oil and gas producing areas: Association of Petroleum Geochemical Explorationists Bulletin, v. 3, p. 114-134.

Foote, R.S., 1996, Relationship of near-surface magnetic anomalies to oil- and gas-producing areas, *in* D. Schumacher and M.A. Abrams, eds., Hydrocarbon migration and its near-surface expression: AAPG Memoir 66, p. 111-125.

Foote, R.S., and G.J. Long, 1988, Correlations of oil- and gas- producing areas with magnetic properties of the upper rock column, eastern Colorado: Association of Petroleum Geochemical Explorationists Bulletin, v. 4, p. 47-61.

Fredrickson, J.K., and Y.A. Gorby, 1996, Environmental processes mediated by iron-reducing bacteria: Biotechnology, v. 7, p. 287-294.

Fredrickson, J.K. et al., 1998, Biogenic iron mineralization accompanying the dissimilatory reduction of hydrous ferric oxide by a groundwater bacterium: Geochimica et Cosmochimica Acta, v. 62/19/20, p. 3239-3257.

Fredrickson, J.K. et al., 2000, Reduction of U (VI) in goethite (alpha-FeOOH) suspensions by a dissimilatory metal-reducing bacterium: Geochimica et Cosmochimica Acta, v. 64/18, p. 3085-3098.

Gay, J.S.P., 1992, Epigenetic versus syngenetic magnetite as a cause of magnetic anomalies: Geophysics, v. 57, p. 60-68.

Gay, J.S.P., and B.W. Hawley, 1991, Syngenetic magnetic anomaly sources: three examples: Geophysics, v. 56, p. 902-913.

Glasauer, S., P.G. Weidler, S. Langley, and T.J. Beveridge, 2003, Controls on Fe reduction and mineral formation by a subsurface bacterium: Geochimica et Cosmochimica Acta, v. 677, p. 1277-1288.

Goldhaber, M.B., R.L. Reynolds, and R.O. Rye, 1978, Origin of a South Texas roll-type uranium deposit, II: sulfide petrology and sulfur isotope studies: Economic Geology, v. 73, p. 1690-1703.

Goldhaber, M.B., R.L. Reynolds, and R.O. Rye, 1983, Role of fluid mixing and fault-related sulfide in the origin of the Ray Point uranium district, south Texas. Economic Geology, v. 78, p. 1043-1063.

Gómez, J., 2002, Geología-Geomorfología y Fisiografía, Ibagué: Alcaldía Municipal de Atacó Tolima.

Guerrero, J., 1993, Magnetostragraphy of the upper part of the Honda Group and Neiva Formation, Miocene uplift of the Colombian Andes.

Hansel, C.M., and C.J. Lentini, 2011, Mineralogical controls on microbial reduction of Fe(III) (Hydro)oxides, *in* J.F. Stolz and R.S. Oremland, eds., Microbial Metal and Metalloid Metabolism, Advances and Applications: American Society for Microbiology (ASM).

Harker, A., 1909, The Natural History of Igneous Rocks: Methuen and Co., London.

Heemstra, R.J. et al., 1979, A critical laboratory and field evaluation of selected surface prospecting techniques for locating oil and natural gas: Bartlesville Energy Technology Center, Bartlesville, Oklahoma, p. 84.

Harris, G.D., 1908, Salt in Louisiana, with special reference to its geologic occurrence, part II--Localities south of the Oligocene: Louisiana Geological Survey Bulletin, v. 7, p. 18-27.

Henry, W.E., 1988, Magnetic detection of hydrocarbon microseepage in a frontier exploration region: Association of Petroleum Geochemical Explorationists Bulletin, v. 4, p. 18-29.

Hettner, 1892, Die Kordillere von Bogotá: Peterm. Mitt. Erg-Bd, v. 104/22, p. 131.

Horvitz, L., 1945, Recent developments in geochemical prospecting for petroleum: Geophysics, v. 10, p. 487-493.

Horvitz, L., 1985, Geochemical exploration for petroleum: Science, v. 229, p. 821-827.

Hovland, M.T., and A.G. Judd, 1988, Seabed pockmarks and seepages: impact on geology, biology, and the marine environment: Graham and Trotman, London, 293 p.

Hughes, L.J., K.L. Zonge, and N.R. Carlson, 1986, The application of electrical techniques in mapping hydrocarbon-related alteration: Southern Methodist University Press Dallas, Texas, p. 5-26.

IGAC, 2004, Descripción de los Suelos, Estudio General de Suelos y Zonificación de Tierras del Departamento de Tolima, Ibagué, Colombia, Instituto Geográfico Agustín Codazzi, p. 29-110.

Jaramillo, J.M., 1980, Chemical Composition, *in* Petrology and Geochemistry of the Nevado Del Ruiz Volcano, Northern Andes, Colombia: University of Houston, Houston, Texas, p. 69-119.

Jaramillo, J.M., 1980, Petrography and mineral composition, petrography and geochemistry of the Nevado Del Ruiz Volcano, Northern Andes, Colombia: University of Houston, Houston, Texas, p. 21-63.

Kartsev, A.A., Z.A. Tabasaranskii, M.I. Subbota, and G.A. Mogilevskii, 1959, Geochemical methods of prospecting and exploration for petroleum and natural gas: University of California Press, Berkeley, CA, 349 p..
Keating, P., and P. Sailhac, 2004, Use of the analytic signal to identify magnetic anomalies due to kimberlite pipes: Geophysics, v. 39, p. 180-190.

Kelly, S.D., 2010, Uranium Chemistry in Soils and Sediments, Synchrotron-Based Techniques in Soils and Sediments: Elsevier, Argonne, Illinois, p. 411-466.

Kennicutt, M.C. et al., 1985, Vent-type taxa in a hydrocarbon seep region of the Louisiana slope: Nature, v. 317, p. 351-353.

Klusman, R.W., 1993, Soil gas and related methods for natural resource exploration: Chichester, John Wiley and Sons, Chichester, England.

Kostka, J.E., and S.J. Green, 2011, Microorganisms and processes linked to uranium reduction and immobilization, *in* J.F. Stolz and R.S. Oremland, eds., Microbial Metal and Metalloid Metabolism: Advances and Applications: American Society for Microbiology Press, Washington.

Koyuncu, H., 1992, Spectral remote sensing of anomalous mineralogy induced by hydrocarbon migration and uranium mineralization, San Rafael Swell, Utah, USA, *in* Remote Sensing for Environmental Monitoring and Resource Management, European International Space Year Conference, Munich, Germany, 30 March-4 April, European Space Agency, p. 455-460.

Krumbein, W.E., 1983, Microbial geochemistry: Alden Press, Oxford, 330 p.

Lilburn, R.A., and Al-Shaieb, Z., 1983, Geochemistry and isotopic composition of hydrocarbon-induced diagenetic aureole (HIDA), Cement, Oklahoma: Oklahoma City Geological Society Shale Shaker, pt. I, v. 34/4, p. 40-56.

Lilburn, R.A., and Al-Shaieb, Z., 1984, Geochemistry and isotopic composition of hydrocarbon-induced diagenetic aureole (HIDA), Cement, Oklahoma: Oklahoma City Geological Society Shale Shaker, pt. II, 34/5, p. 57-67.

Liu, X.-M., J. Bloemendal, and T. Rolph, 1994, Pedogenesis and paleoclimate: interpretations of the magnetic susceptibility record of Chinese loess-paleosol sequences, comment: Geology, v. 22, p. 858-859.

Lovley, D., 1993, Dissimilatory metal reduction: Annu. Rev. Microbiol., v. 47, p. 263-290.

MacDonald, I.R. et al., 1989, Gulf of Mexico hydrocarbon seep communities: Marine Geology, v. 101, p. 235-247.

MacDonald, I.R. et al., 1990, Chemosynthetic mussels at a brine-filled pockmark in the northern Gulf of Mexico: Science, v. 248, p. 1096-1099.

Machel, H.G., 1996, Magnetic Contrasts as a Result of Hydrocarbon Seepage and Migration, *in* D. Schumacher and M.A. Abrams, eds., Hydrocarbon migration and its near-surface expression. AAPG Memoir 66, p. 99-109.

Machel, H.G., and E.A. Burton, 1991a, Chemical and microbial processes causing anomalous magnetization in environments affected by hydrocarbon seepage: Geophysics, v. 56, p. 598-605.

Machel, H.G., and E.A. Burton, 1991b, Causes and spatial distribution of anomalous magnetization in hydrocarbon seepage environments: AAPG Bulletin, v. 75, p. 1864-1876.

MacLeod, I., K. Jones, and T. Dai, 1993, 3-D analytic signal in the interpretation of total magnetic field data at low magnetic latitudes: Exploration Geophysics, v. 24, p. 679-688.

Maher, B.A., and R. Thompson, 1991, Mineral magnetic record of the Chinese loess and paleosols: Geology, v. 19, p. 3-6.

Maher, B.A., and R. Thompson, 1992, Paleoclimatic significance of the mineral magnetic record of the Chinese loess and paleosols: Quaternary Research, v. 37, p. 155-170.

Matthews, M.D., 1986, The effects of hydrocarbon leakage on earth surface materials: Southern Methodist University Press, Dallas, Texas, p. 27-44.

McCabe, C., R. Sassen, and B. Saffer, 1987, Occurrence of secondary magnetite within biodegraded oil: Geology, v. 15, p. 1351-1370.

McDermott, E., 1940, Geochemical exploration (soil analysis), with speculation about the genesis of oil, gas, and other mineral accumulations: AAPG Bulletin, v. 24, p. 859-881.

McDonough, W., and S.-s. Sun, 1995, The composition of the Earth: Chemical Geology, v. 120, p. 223-253.

McKenna, E.J., and R.E. Kallio, 1965, The biology of hydrocarbons: Annual Reviews of Microbiology, v. 19, p. 183-208.

Meunier, J.D., P. Landais, and M. Pagel, 1990, Experimental evidence of uraninite formation from diagenesis of uranium-rich organic matter: Geochimica et Cosmochimica Acta, v. 54, p. 809-817.

Milner, H.B., 1925, “Paraffin dirt”: its nature, origin, mode of occurrence, and significance as an indication of petroleum: Mining Magazine, v. 32, p. 73-85.

Miyashiro, A., 1974, Volcanic rock series in island arcs and action continental margins: Am. J. Sci., v. 274, p. 321-355.

Mohamed Falcón, K.J., 2006, Influencia Climática, Diagenética y Antropogénica sobre la Señal Magnética y Geoquímica de los Sedimentos Marinos Cuaternarios del Noroeste de la Península Ibérica, Vigo, España: Tesis doctoral, Universidad de Vigo.

Montes, C., 2001, Three dimensional structure and kinematics of the Piedras-Girardot foldbelt in the northern Andes of Colombia: PhD Thesis, The University of Tennessee, p. 201.

Nabighian, M.N., 1972, The analytic signal of two dimensional magnetic bodies with polygonal cross section: Its properties and use for automated anomaly interpretation: Geophysics, v. 37, p. 507-517.

Nabighian, M.N., 1974, Additional comments on the analytic signal of two-dimensional magnetic bodies with polygonal cross-section: Geophysics, v. 39, p. 85-92.

Nabighian, M.N., 1984, Toward the three-dimensional automatic interpretation of potential field data via generalized Hilbert Transforms: Fundamental relations: Geophysics, v. 53, p. 957-966.

Oehler, D.Z., and B.K. Sternberg, 1984, Seepage-induced anomalies, "false" anomalies, and implications for electrical prospecting: AAPG Bulletin, v. 68, p. 1121-1145.

Olmstead, R.W., 1975, Geochemical studies of uranium in south-central Oklahoma: Master's Thesis, Oklahoma State University, Stillwater, Oklahoma, 116 p.

Pardo, A., D. Barrero, C.A. Vargas, and J. F. Martínez, 2007, Geological Framework, *in* ANH & B. & E. Exploration Ltda, eds., Colombian Sedimentary Basins: Nomenclature, Boundaries and Petroleum Geology, A New Proposal, Bogotá: Agencia Nacional de HydrocarbonsColombia, p. 17-21.

Pardo, A., C.A. Vargas, D. Barrero, and J.F. Martínez, 2007, Review of Nomenclature and Boundaries of Colombian Basins, *in* ANH & B. & E. Exploration Ltda, eds., Colombian Sedimentary Basins: Nomenclature, Boundaries and Petroleum Geology, A New Proposal, Bogotá: Agencia Nacional de Hidrocarburos Colombia, p. 22-27, 50.

Phillips, D.J., 2000, Locating magnetic contacts: a comparison of the horizontal gradient, analytic signal, and local wave number methods: 70th SEG Annual International Meeting, Expanded Abstracts with Biografies, Technical Program, v. 1, p. 402-405.

Pirson, S.J., 1969, Geological, geophysical, and geochemical modification of sediments in the environments of oil fields: Southern Methodist University Press, Dallas, Texas, p. 159-186.

Price, L.C., 1986, A critical overview and proposed working model of surface geochemical exploration: Southern Methodist University Press, Dallas, Texas, p. 245-304.
Price, L.C., 1996, Research-Derived Insights into Surface Geochemical Hydrocarbon exploration, *in* D. Schumacher and M.A. Abrams, eds., Hydrocarbon migration and its near-surface expression: AAPG Memoir 66, Geologists, p. 285-307.

Reeves, F., 1922, Geology of the Cement oil field, Caddo county, Oklahoma: USGS Bulletin 726, p. 41-85.

Reid, J.C., B.S. Campbell, and S.D. Ulrich, 1992, Hydrocarbon-induced mineralogic and geochemical alteration, Turkey Creek, Colorado: Association of Petroleum Geochemical Explorationists Bulletin, v. 8, p. 64-95.

Reilly, J.F., J.I.R. MacDonald, E.K. Biegret, and J.M. Brooks, 1996, Geologic Controls on the Distribution of Chemosynthetic Communities in the Gulf of Mexico, *in* D. Schumacher and M.A. Abrams, eds., Hydrocarbon migration and its near-surface expression: AAPG Memoir 66, p. 39-61.

Reynolds, R.L., N.S. Fishman, R.I. Grauch, and J.A. Karachewski, 1984, Thermomagnetic behavior and composition of pyrrhotite in Lower Permian strata, Cement oil field, Oklahoma: EOS Transactions, American Geophysical Union, v. 6545, p. 866.

Reynolds, R.L., N.S. Fishman, and D.M. Sherman, 1988, Magnetite and maghemite from hydrocarbon wells: EOS Transactions American Geophysical Union, v. 65/44, p. 1156.

Reynolds, R.L., N.S. Fishman, R.B. Wanty, and M.B. Goldhaber, 1990, Iron sulfide minerals at Cement oil field, Oklahoma: implications for magnetic detection of oil fields: GSA Bulletin, v. 102, p. 368-380.

Reynolds, R.L., M.B. Goldhaber, and M.L. Tuttle, 1993, Sulfidization and magnetization above hydrocarbon reservoirs, *in* D.M. Aissaoui, D.S. McNeill, and N.F. Hurley, eds., Application of paleomagnetism to sedimentary geology: SEPM Special Publication 49, p. 167-179.

Rosaire, E.E., 1940, Geochemical prospecting for petroleum; AAPG Bulletin, v. 24, p. 1400-1423.

Santacruz, C., 2014, Análisis de la Relación entre los Sistemas de Levantamiento y la Precipitación de Orgánicos en los Pozos de los Campos Maná y Toqui de la Cuenca del Valle Superior del Magdalena.

Sassen, R., E.W. Chinn, and C. McCabe, 1988, Recent hydrocarbon alteration, sulfate reduction, and formation of elemental sulfur and metal sulfides in salt dome cap rock: Chemical Geology, v. 74, p. 57-66.

Sassen, R., C.M. McCabe, J.R. Kyle, and E.W. Chinn, 1989, Deposition of magnetic pyrrhotite during alteration of crude oil and reduction of sulfate: Organic Geochemistry, v. 14, p. 381-392.

Sassen, R. et al., 1993, Chemosynthetic bacterial mats at cold hydrocarbon seeps, Gulf of Mexico continental slope: Organic Geochemistry, v. 20, p. 77-89.

Saunders, D.F., K.R. Burson, J.F. Branch, and C.K. Thompson, 1993, Relation of thorium-normalized surface and aerial radiometric data to subsurface petroleum accumulations: Geophysics, v. 58, p. 1417-1427.

Saunders, D.F., K.R. Burson, and C.K. Thompson, 1991, Observed relation of soil magnetic susceptibility and soil gas hydrocarbon analysis to subsurface petroleum accumulations: AAPG Bulletin, v. 75, p. 389-408.

Sawtelle, G., 1936, Salt dome statistics: AAPG Bulletin, v. 20, p. 726-735.

Schumacher, D., 1996, Hydrocarbon-Induced Alteration of Soils and Sediments, *in* D. Schumacher and M.A. Abrams, eds., Hydrocarbon Migration and Its Near-Surface Expression: AAPG Memoir 66, p. 71-89.

SGC, 2015, Plancha 5-09 del Atlas Geológico de Colombia, Escala 1:500 000, *in* J. Gómez, N.E. Montes, Á. Nivia, and H. Diederix, eds., Mapa Geológico Colombiano: Bogotá: Servicio Geológico Colombiano.

Spirakis, C.S., 1996, The roles of organic matter in the formation of uranium deposits in sedimentary rocks: Ore Geology Reviews, v. 8, p. 53-69.

Sternberg, B.K., 1991, A review of some experience with the induced polarization-resistivity method for hydrocarbon surveys: successes and limitations: Geophysics, v. 56, p. 1522-1532.

Thompson, A.B., 1933, The economic value of surface petroleum manifestations: First World Petroleum Congress, Proceedings, p. 241-150.

Thompson, C.K., D.F. Saunders, and K.R. Burson, 1994, Model advanced for hydrocarbon microseepage, related alterations: Oil and Gas Journal, November 14, p. 95-99.

Ville, J., 1948, Theorie et applications de la notion de signal analytique: Cables et Transmissions, v. 712, p. L13-L16.

Weart, R.C. and, G. Heimberg, 1981, Exploration radiometrics: post-survey drilling results, *in* M.J. Davidson and B. M. Gottlieb, eds., Unconventional methods in exploration for petroleum and natural gas, Symposium II: Southern Methodist University Press, Dallas, Texas, p. 116-123.

Wilkins, M.J., F.R. Livens, D.J. Vaughan, and J.R. Lloyd, 2006, The impact of Fe(III)-reducing bacteria on uranium mobility: Biogeochemistry, v. 78, p. 125-150.

Zhang, C. et al., 1997, Physiochemical, mineralogical, and isotopic characterization of magnetite-rich iron oxides formed by thermophilic iron-reducing bacteria: Geochimica et Cosmochimica Acta, v. 61/21, p. 4621-4632.

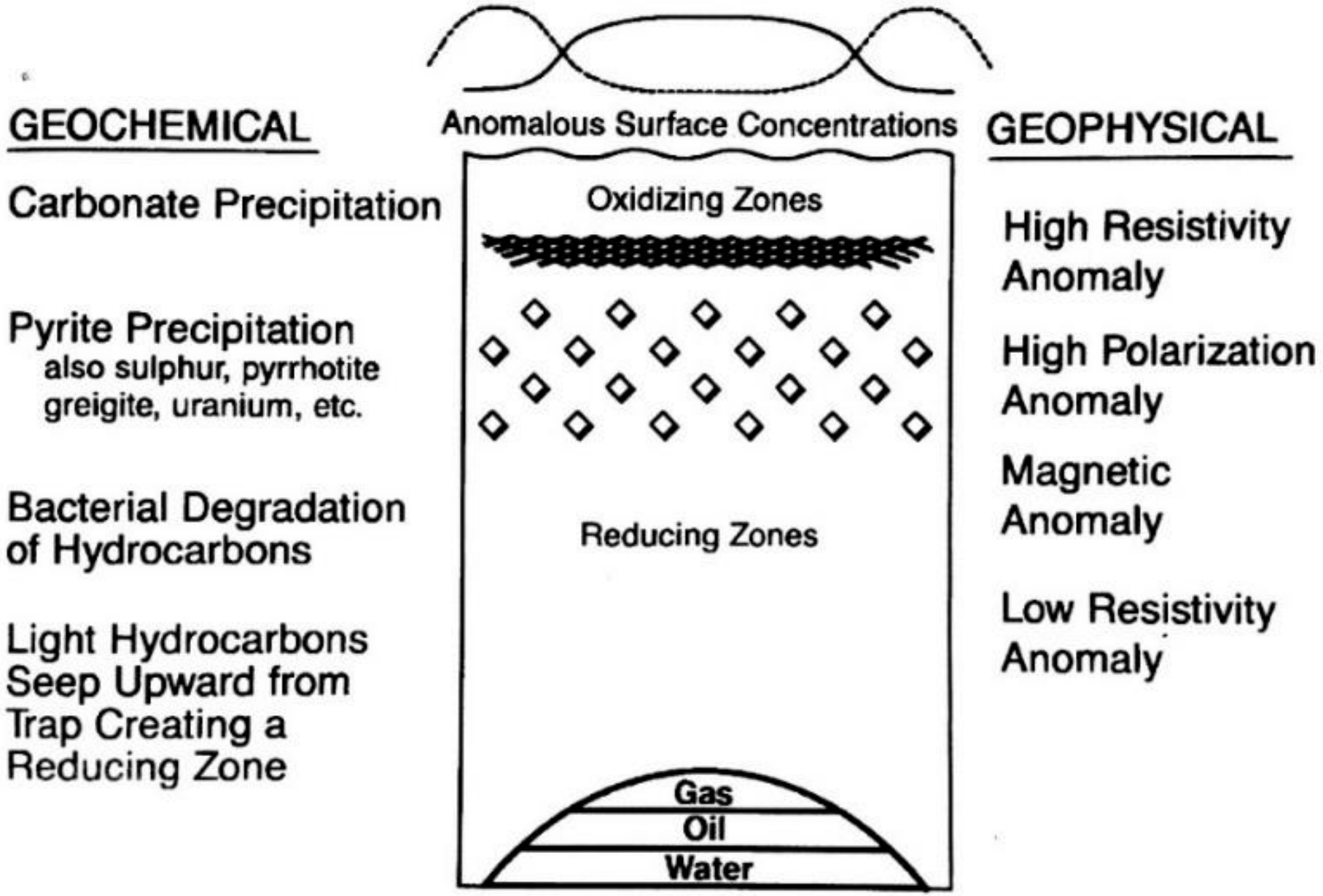

Figure 1. Generalized model of hydrocarbon-induced geochemical and geophysical alteration of soils and sediments. Taken from Schumacher, 1996.

Figure 2. Location of Piedras Town in Colombia, in Tolima Department. The blue point corresponds to the location of Toqui-Toqui and Maná fields. Modified from Alcaldía de Piedras-Tolima, 2009.

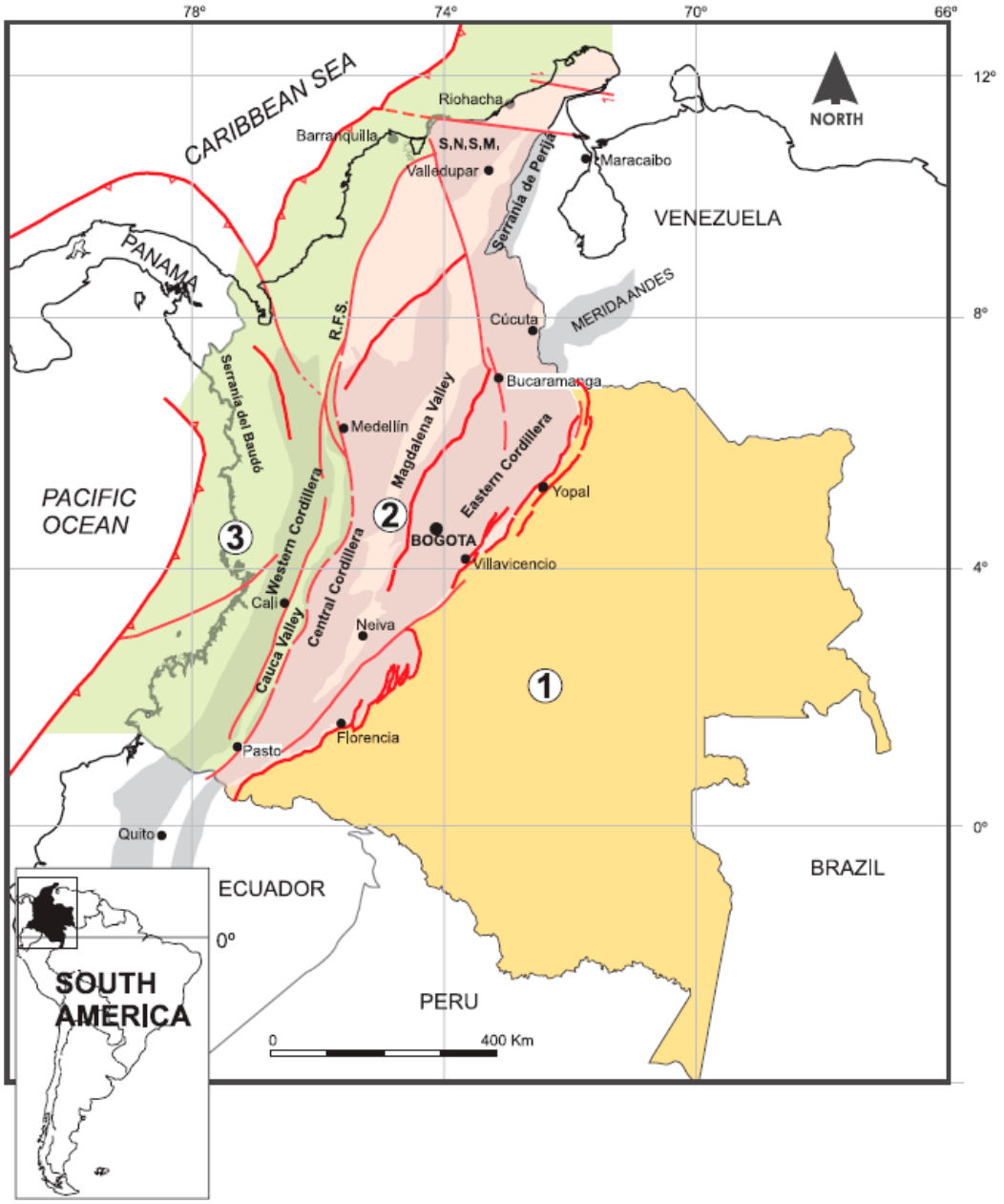

Figure 3. Map of Colombia with its main tectonic domains. (1) Eastern Region, (2) Central Region, (3) Western Region. Regional faults in red. Main mountain ranges in gray and shadow areas. R.F.S. Romeral Fault system; S.N.S.M. Sierra Nevada de Santa Marta. Deep Marine and Los Cayos basins are not included. Taken from Pardo et al., 2007.

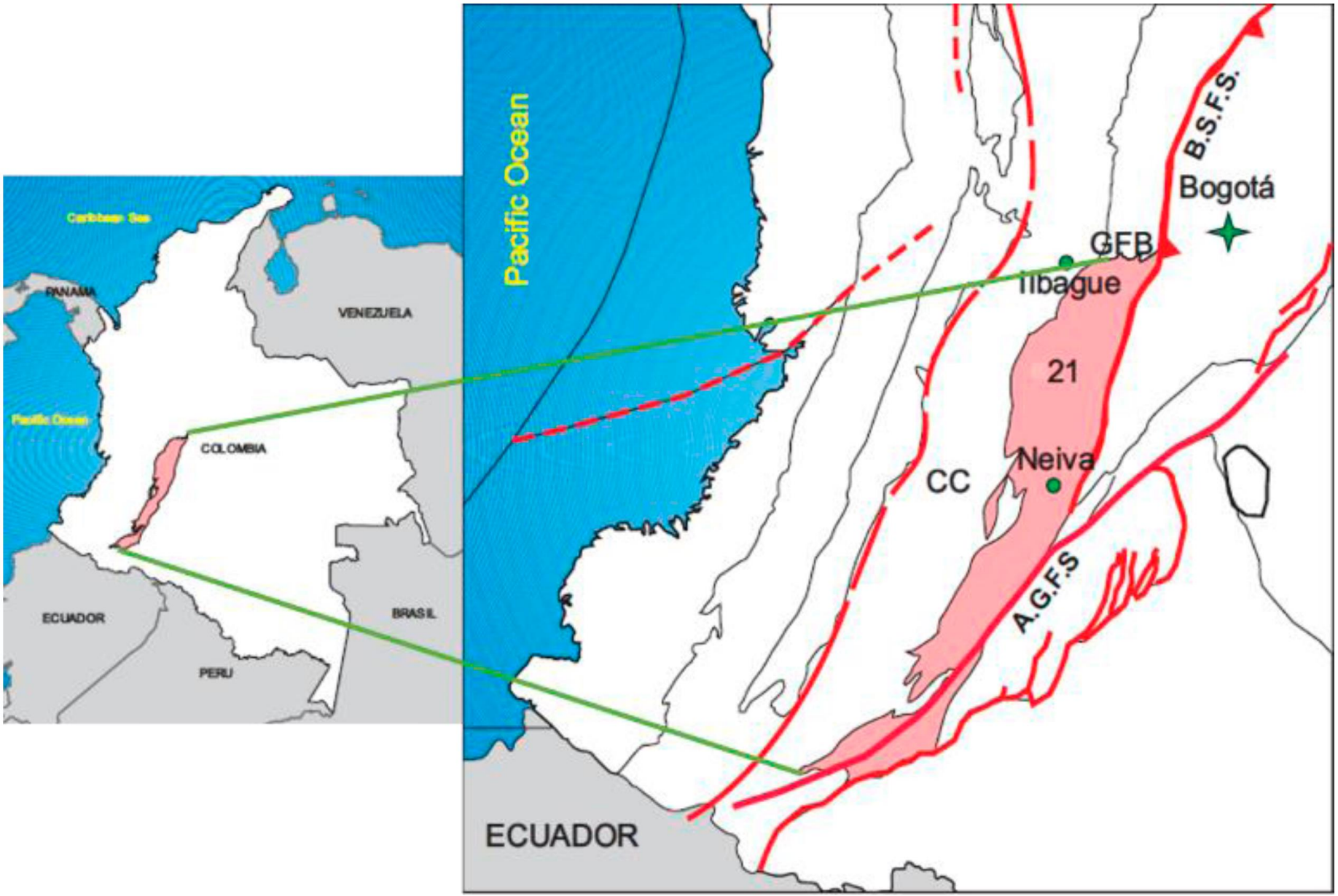

Figure 4. Location of the Upper Magdalena Valley Basin (UMVB). Modified from Pardo et al., 2007.

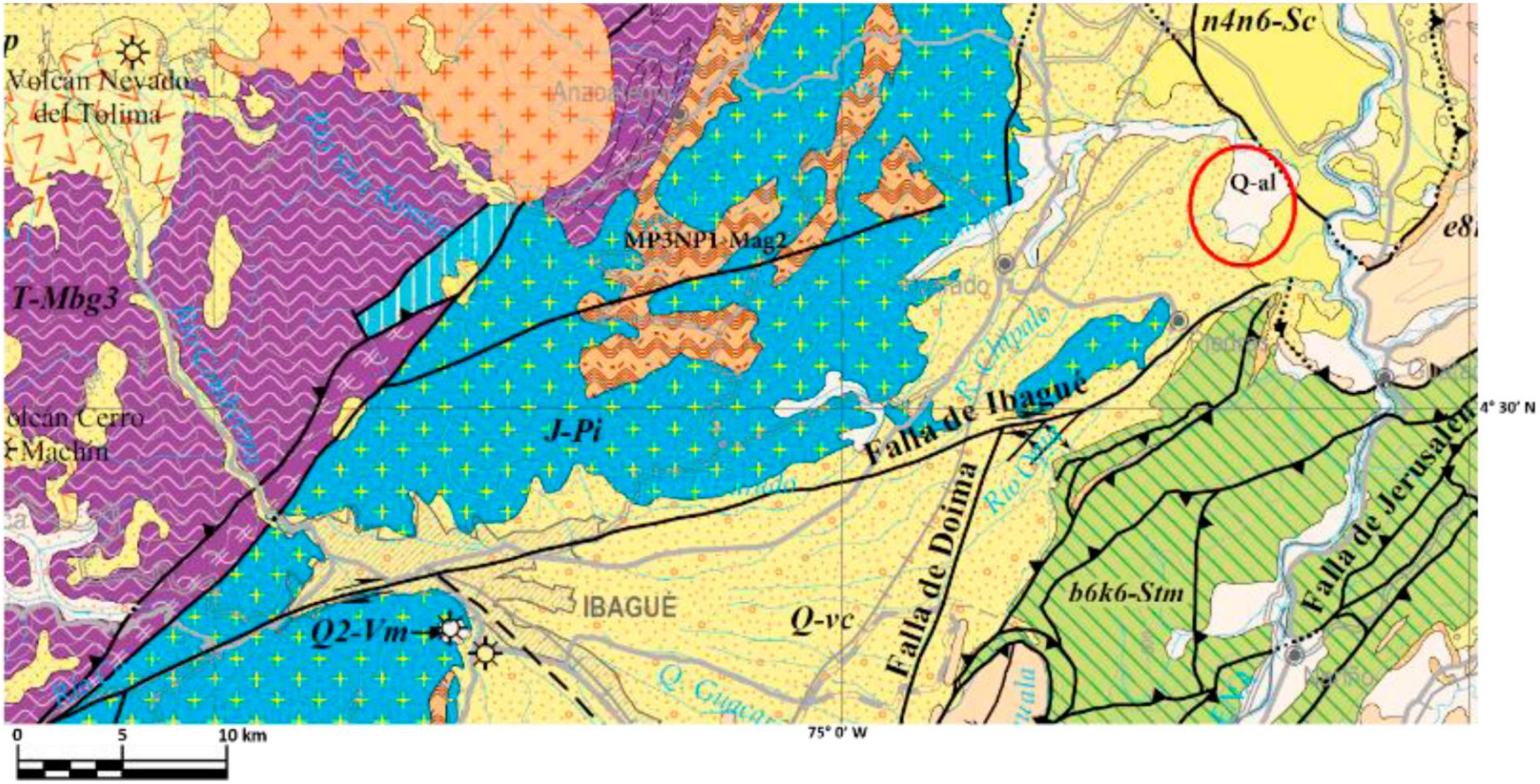

Figure 5. Geological map of the study area and relevant surrounding geological features. Quaternary alluvial deposits (Q-al), Ibagué fan (Q-vc), Honda Fm. (n4n6-Sc), Cretaceous sedimentary rocks (b6k6-Stm), Ibagué Batholite (J-Pi), Triassic metamorphic rocks (T-Mbg3), Mesoproterozoic basement (MP3NP1-Mag2). Toqui-Toqui and Maná fields are inside the red circle. Modified from SGC, 2015.

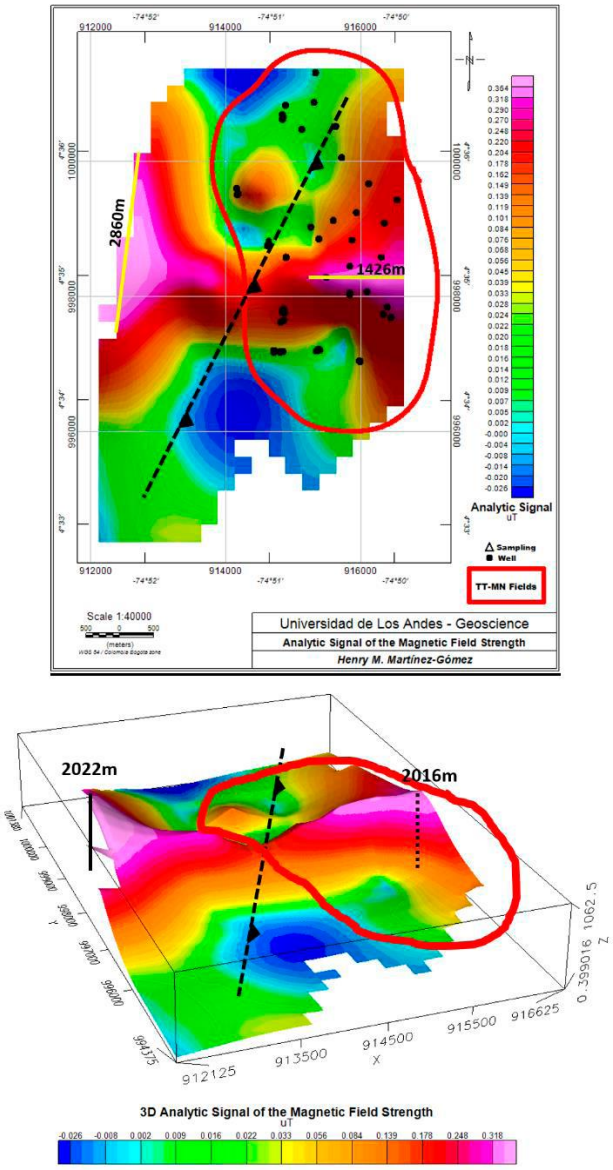

Figure 6. 2D and 3D views of the Analytic Signal of the Magnetic Field Strength. The red line represents the schematic area of Toqui-Toqui and Mana oil fields. Yellow lines represent the extension of the Gaussian bells used to estimate the depth of the sources for the anomalies (i.e. 2022 m depth for the structure on the left side of the map, and 2016 m depth for the structure on the right side of the map). A thrust fault is proposed to be the cause of the discontinuity of the anomalous signal, which is higher on the footwall (i.e. the footwall is deeper than the hanging wall). The source proposed is the Triassic to Jurassic volcanic basement.

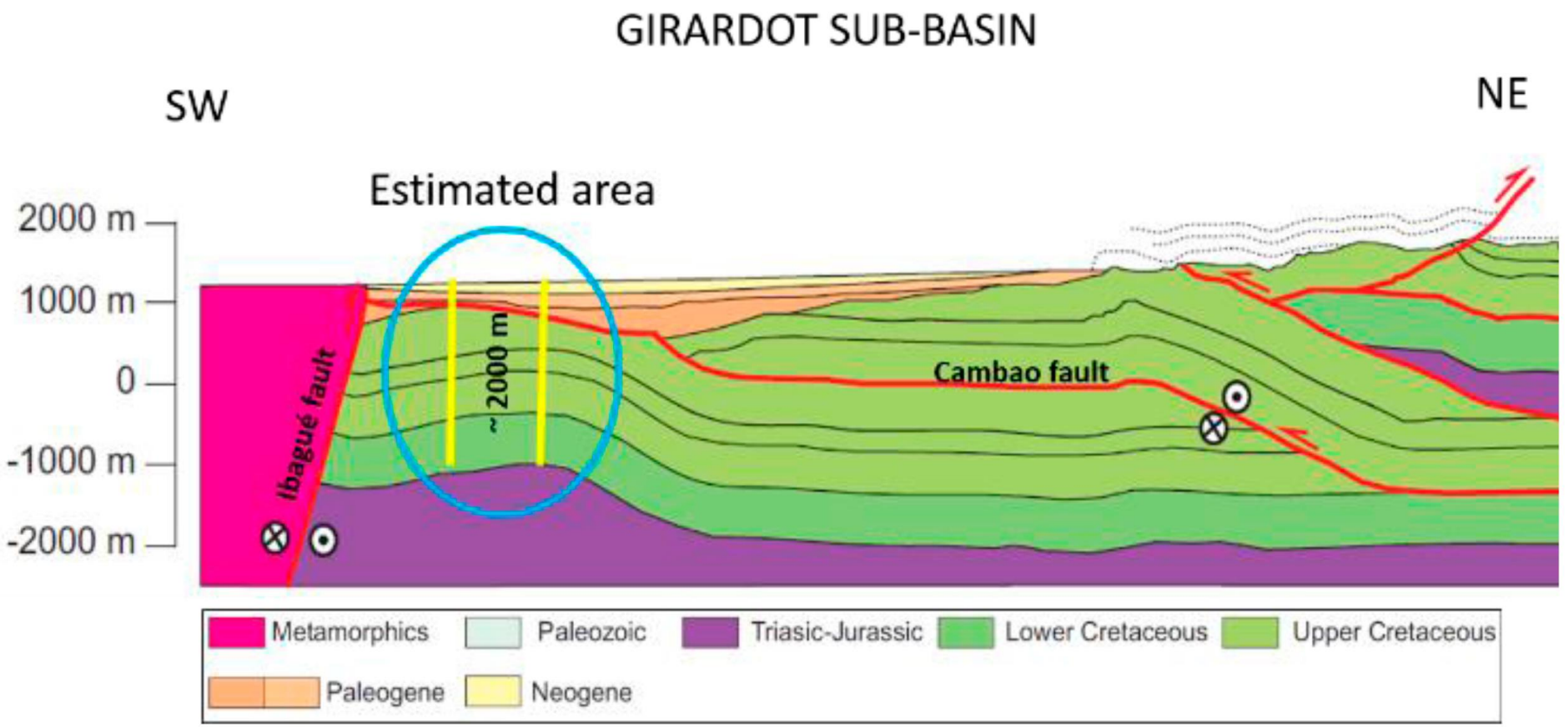

Figure 7. Schematic profile of the Girardot Sub-Basin modified from Montes, 2001. Blue oval represents the estimated area of the map of Analytic Signal. Yellow vertical lines represent the estimated location of the Gaussian bells in the Analytic Signal attributed to the volcanic basement, which are discontinued by Cambao Fault.

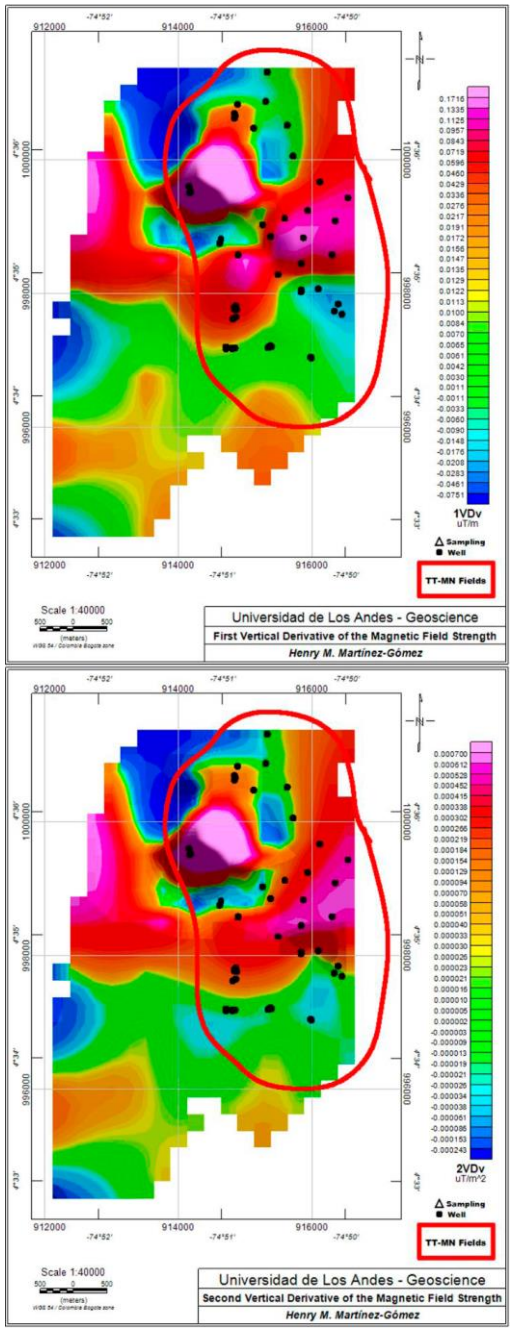

Figure 8. First and Second Vertical Derivatives of the Magnetic Field Strength.

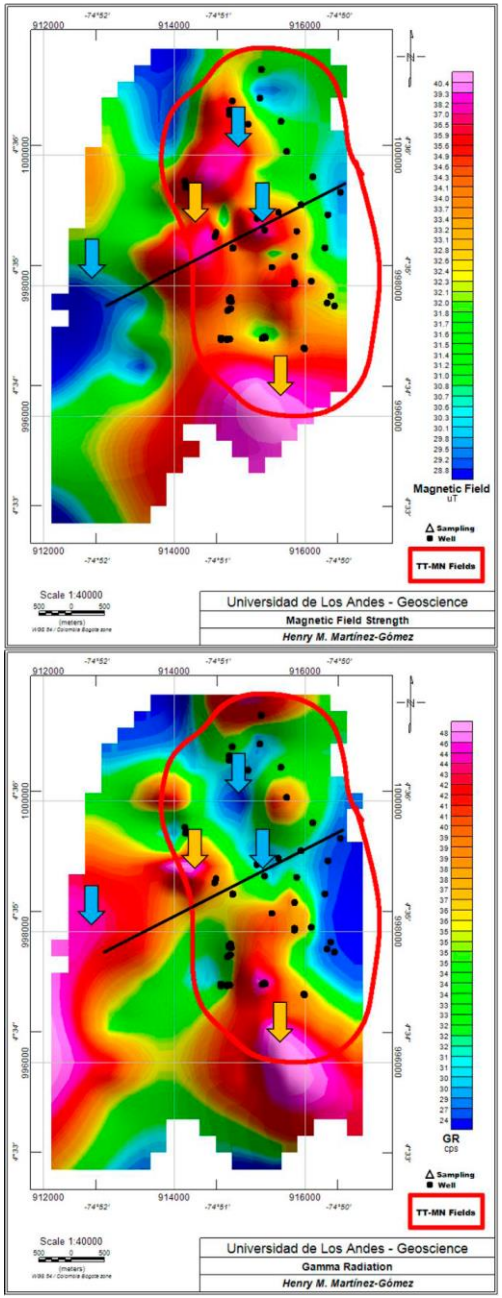

Figure 9. Comparison between Magnetic Field Strength and GR maps. Orange arrows point coincidences. Blue arrows point differences. Black lines are profiles for each geophysical measurement.

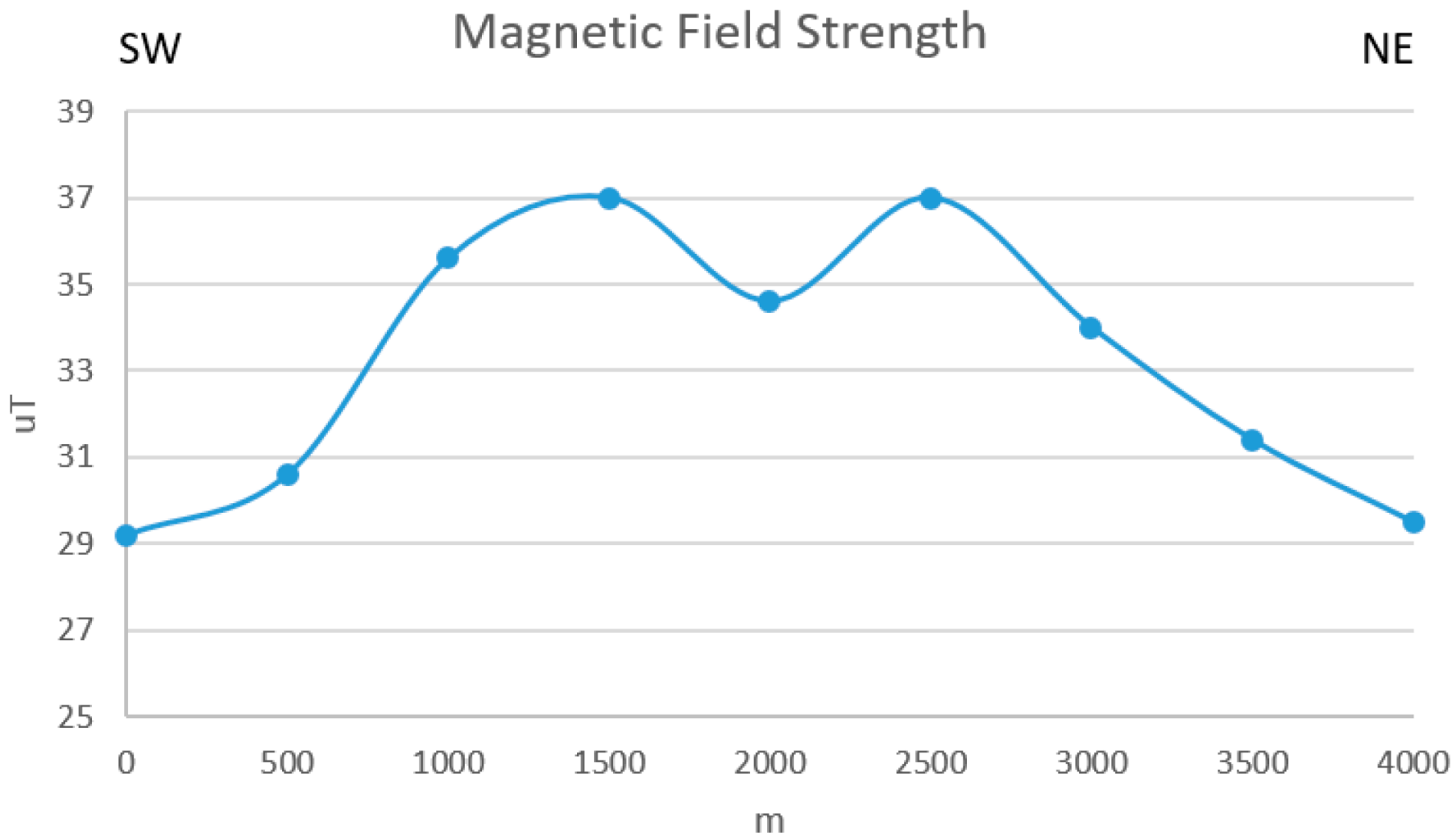

Figure 10. Profile of Magnetic Field Strength measurements, which increase inside Toqui-Toqui and Maná fields.

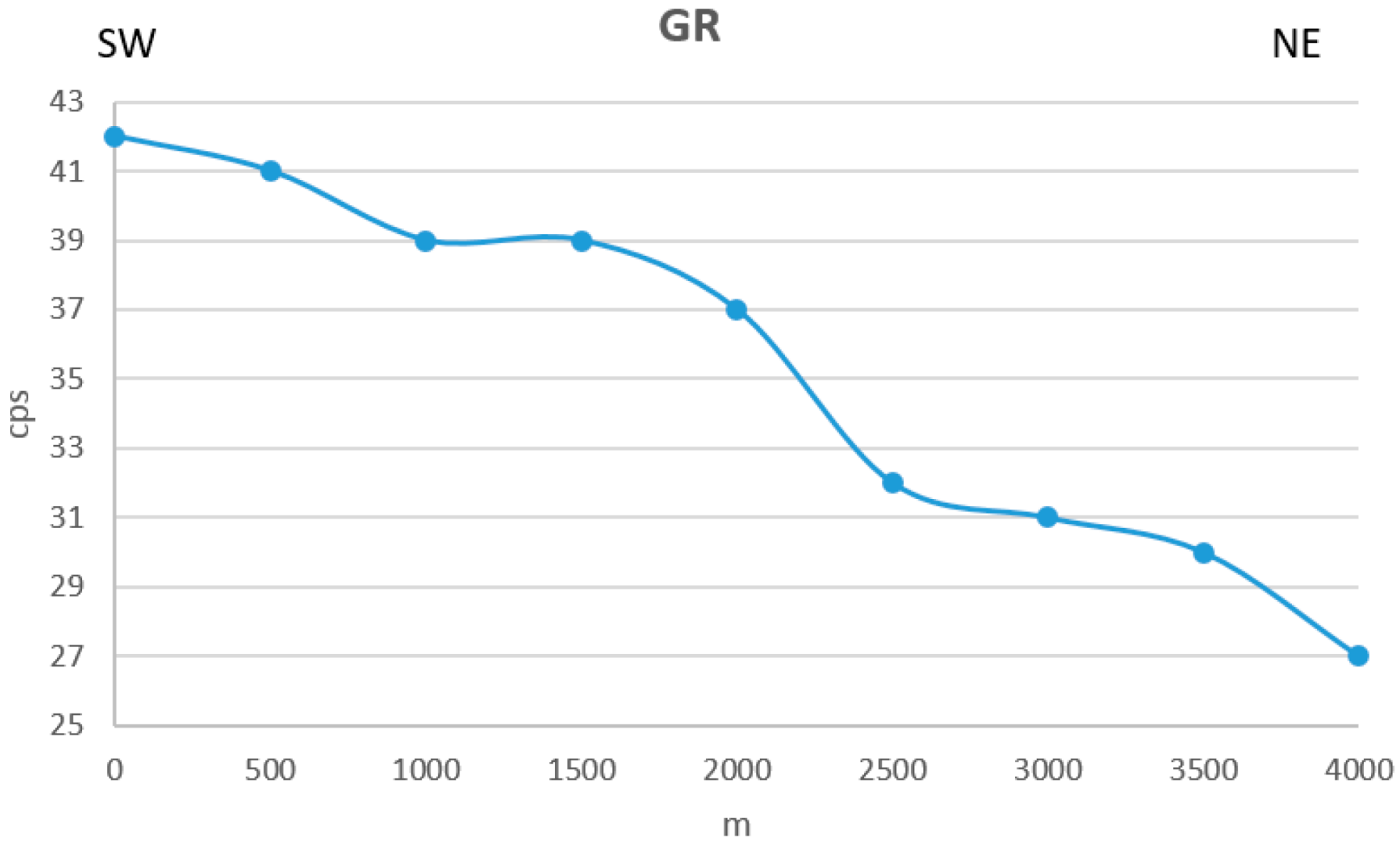

Figure 11. Profile of Gamma Radiation measurements, which are high at the western border of Toqui-Toqui and Maná fields and decreases inside them.

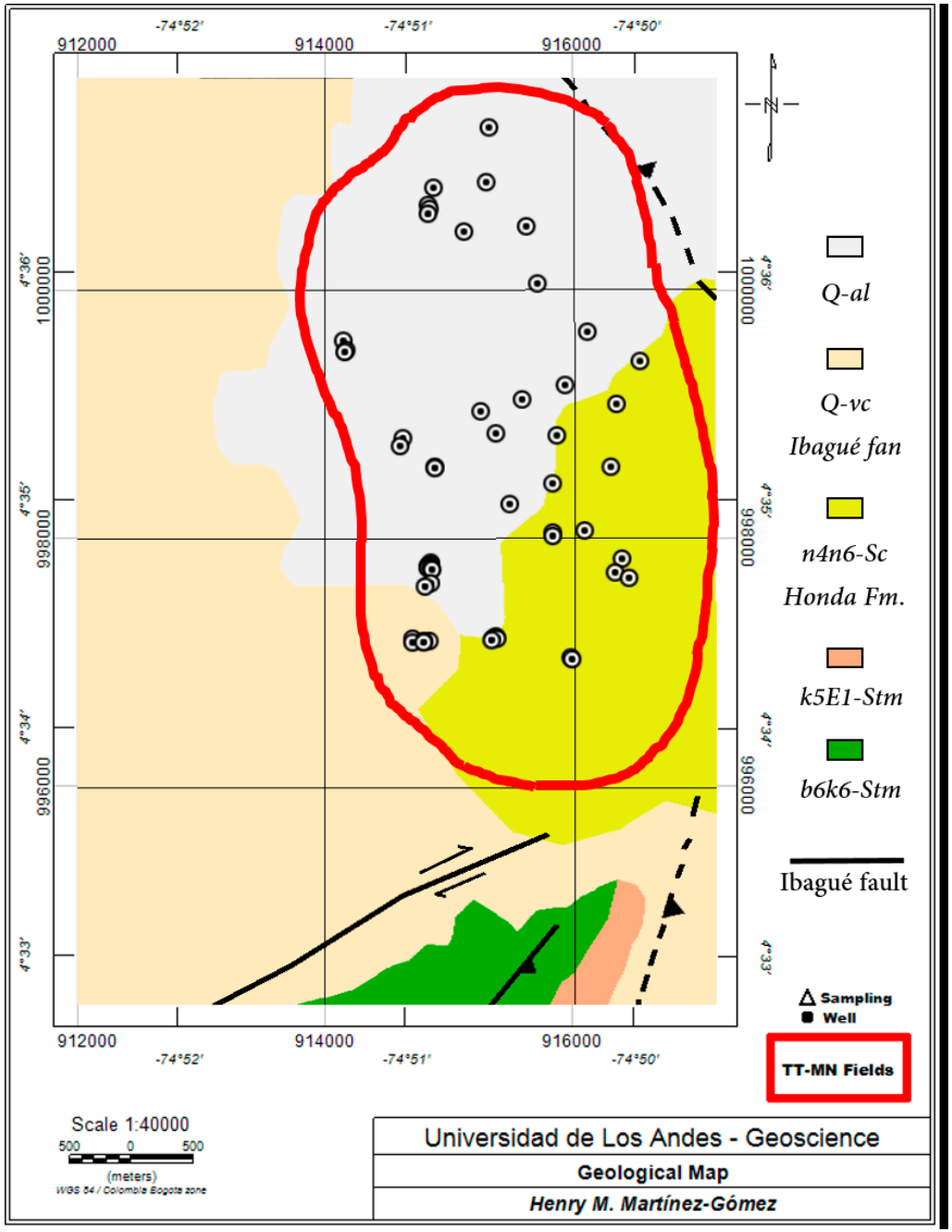

Figure 12. Geological map (adapted from SGC, 2015).

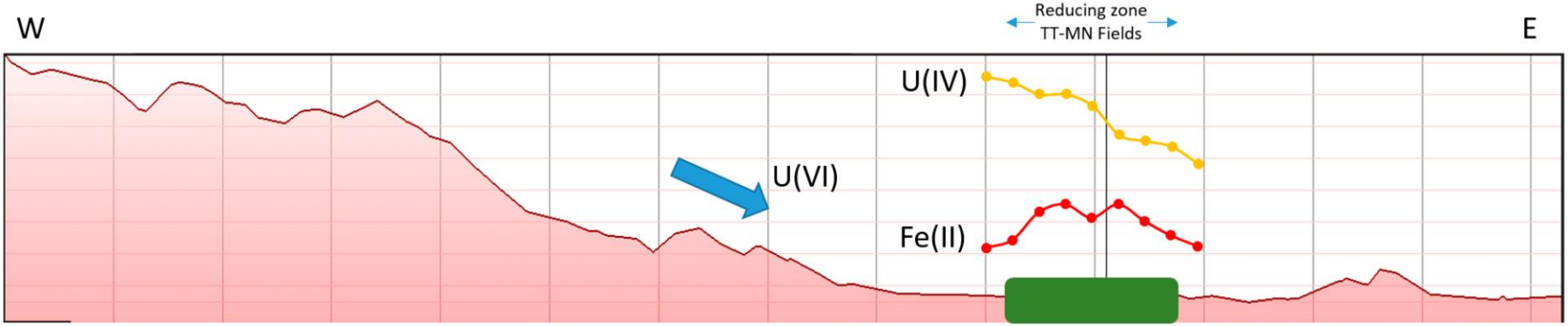

Figure 13. Schematic model of the radiometric and magnetic anomalies over Toqui-Toqui and Maná fields. Soluble U^{6+} goes eastward and precipitates as U^{4+} under the reducing environment produced by TT-MN fields at its western border (i.e. aureole effect), leading to the GR anomaly. U^{6+} and thus U^{4+} decreases to the east, allowing the reduction of the mineralized Fe^{3+} into Fe^{2+}, which generates a magnetic anomaly over TT-MN oil fields (i.e. Gaussian effect).

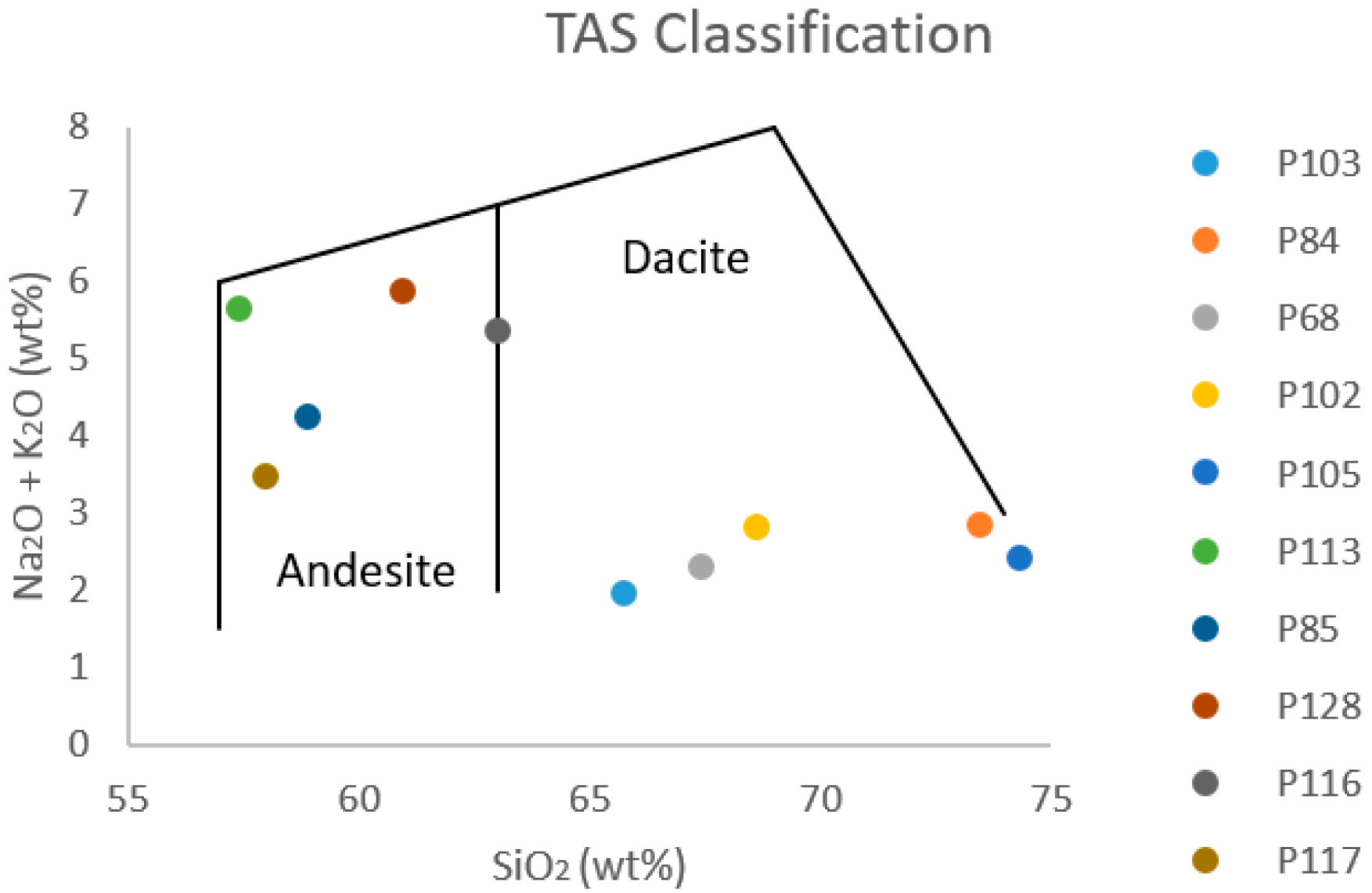

Figure 14. TAS classification for the soil samples. There are 5 samples classified as Andesite and the other 5 as Dacite.

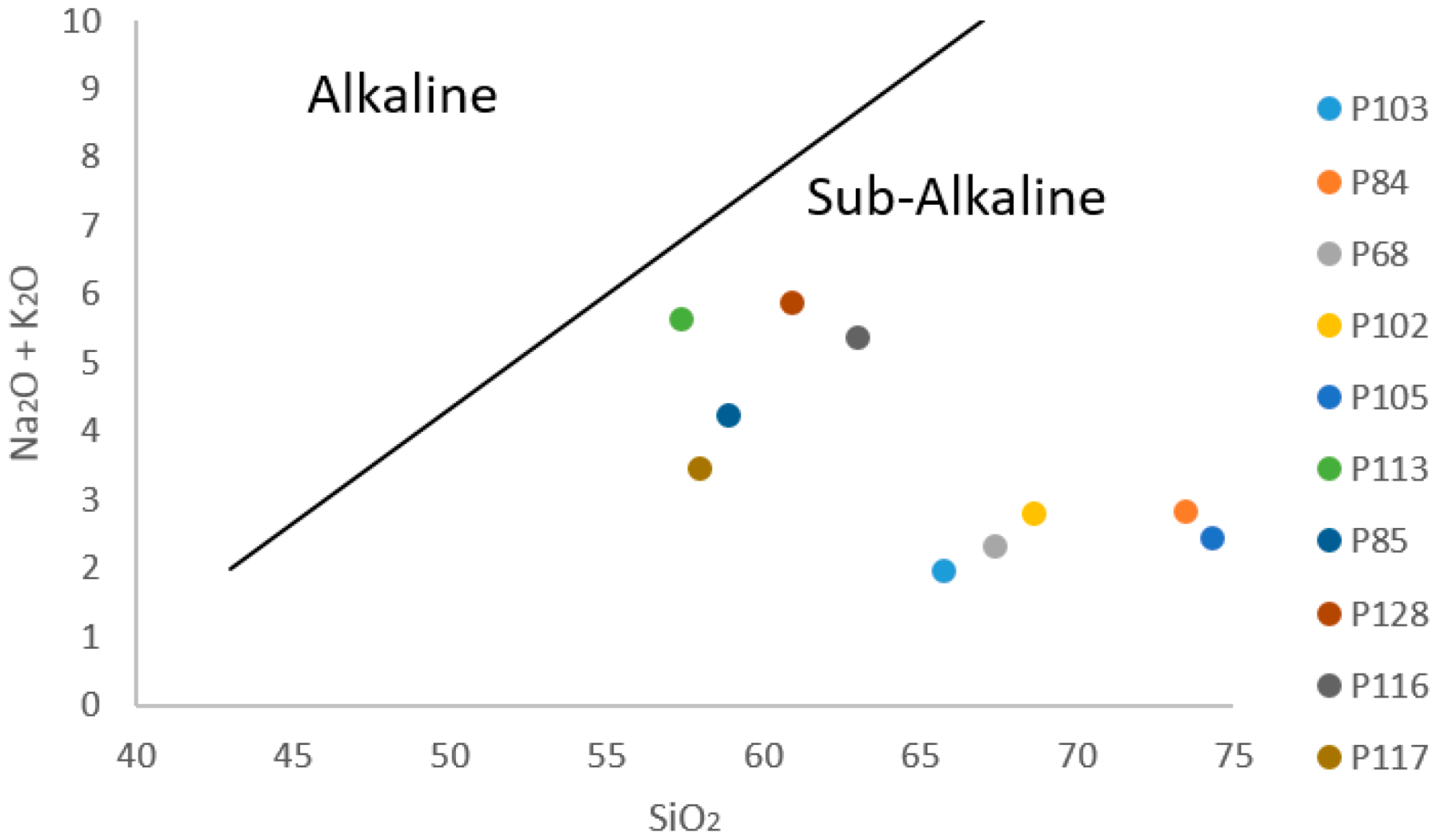

Figure 15. Alkali classification for the soil samples. All the samples plot in the Sub-Alkaline field.

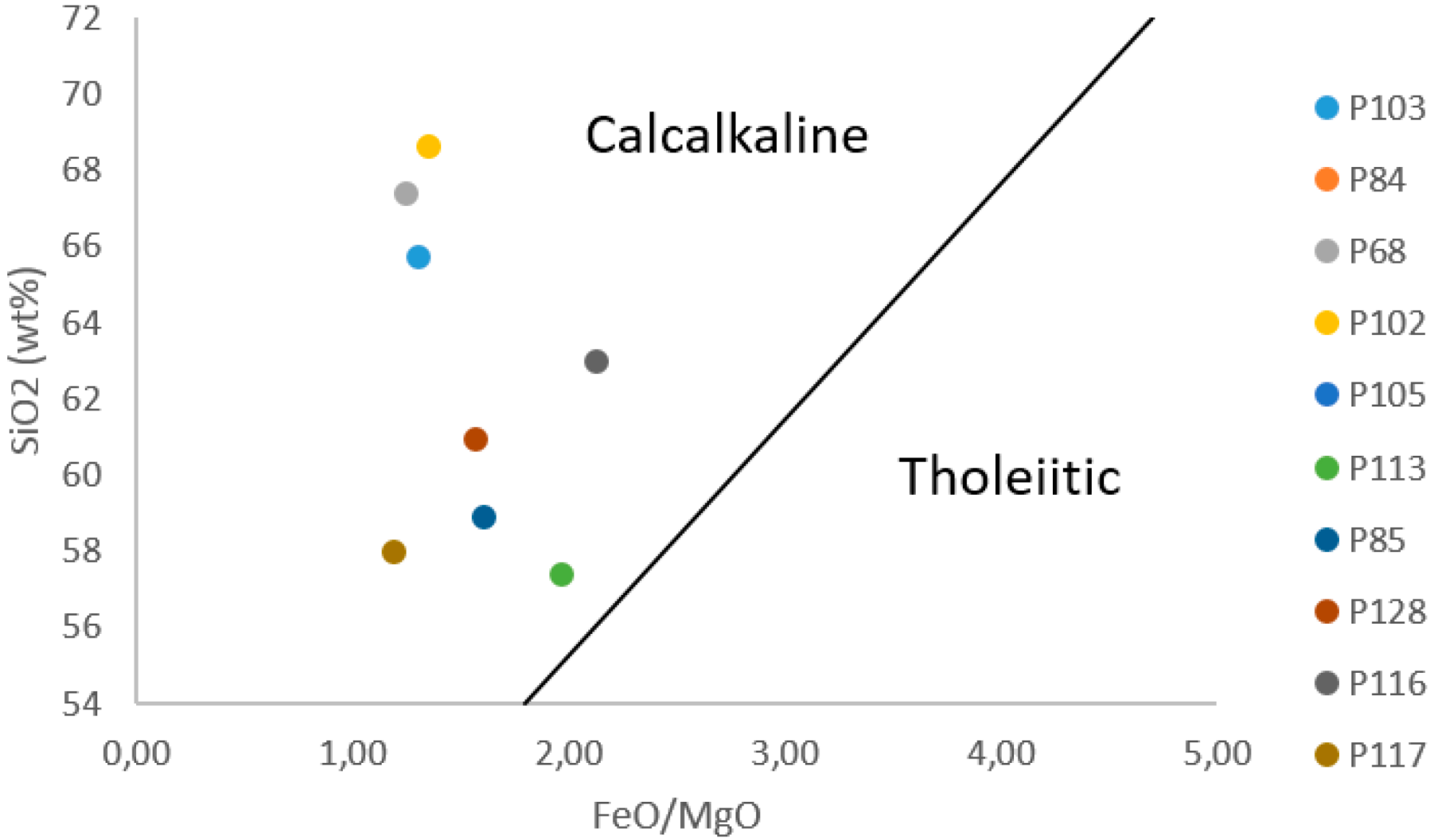

Figure 16. Classification of Sub-Alkaline rocks (Miyashiro, 1974). All the soil samples classify as Calcalkaline.

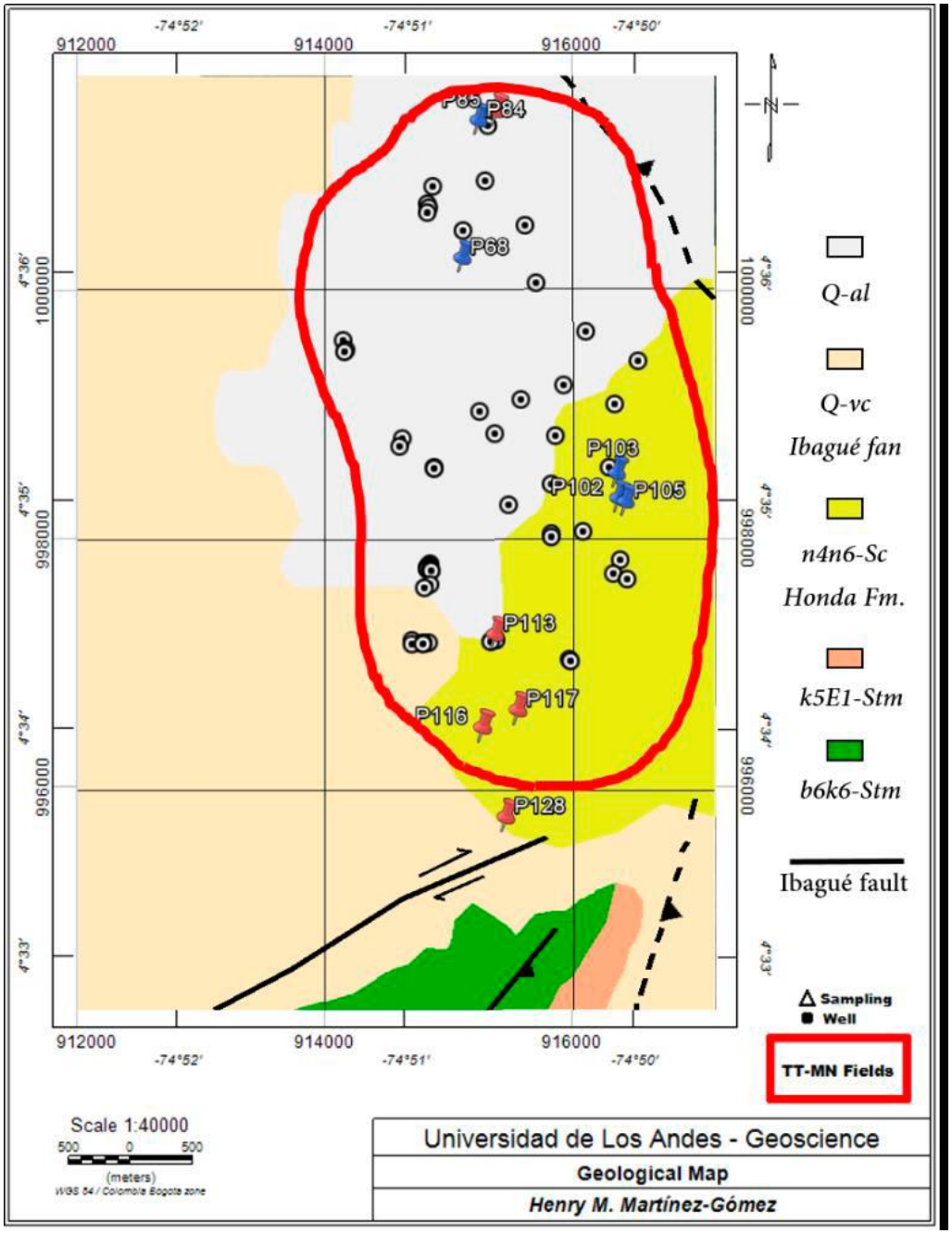

Figure 17. Geological map with the location of the soil samples studied.

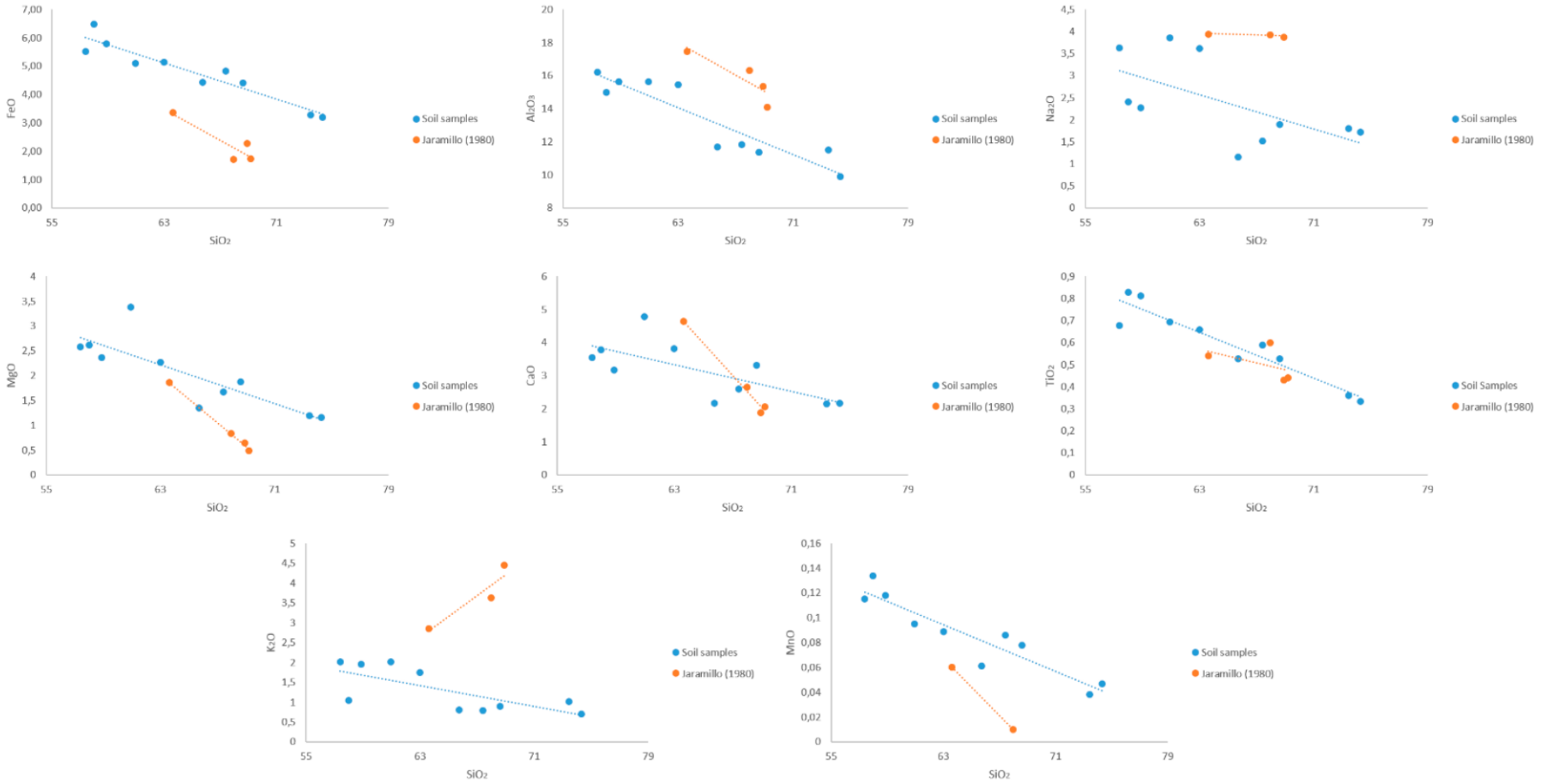

Figure 18. Harker variation diagrams for major elements. Soil samples are compared with data from Jaramillo (1980). Potassium shows anomalous variation.

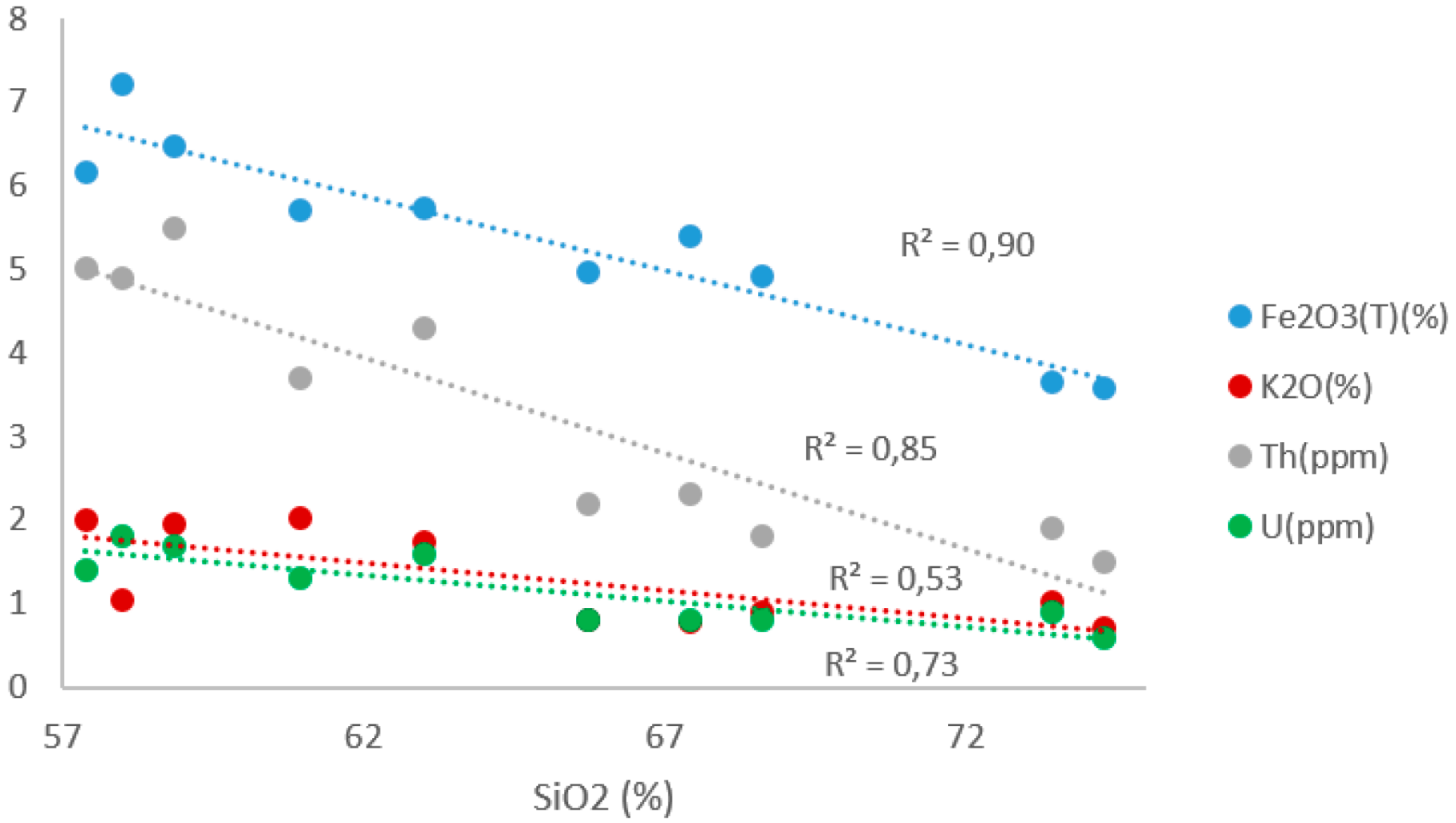

Figure 19. Content of Fe, K, Th and U with respect to the total silica content. Correlation coefficients are shown for each plot.

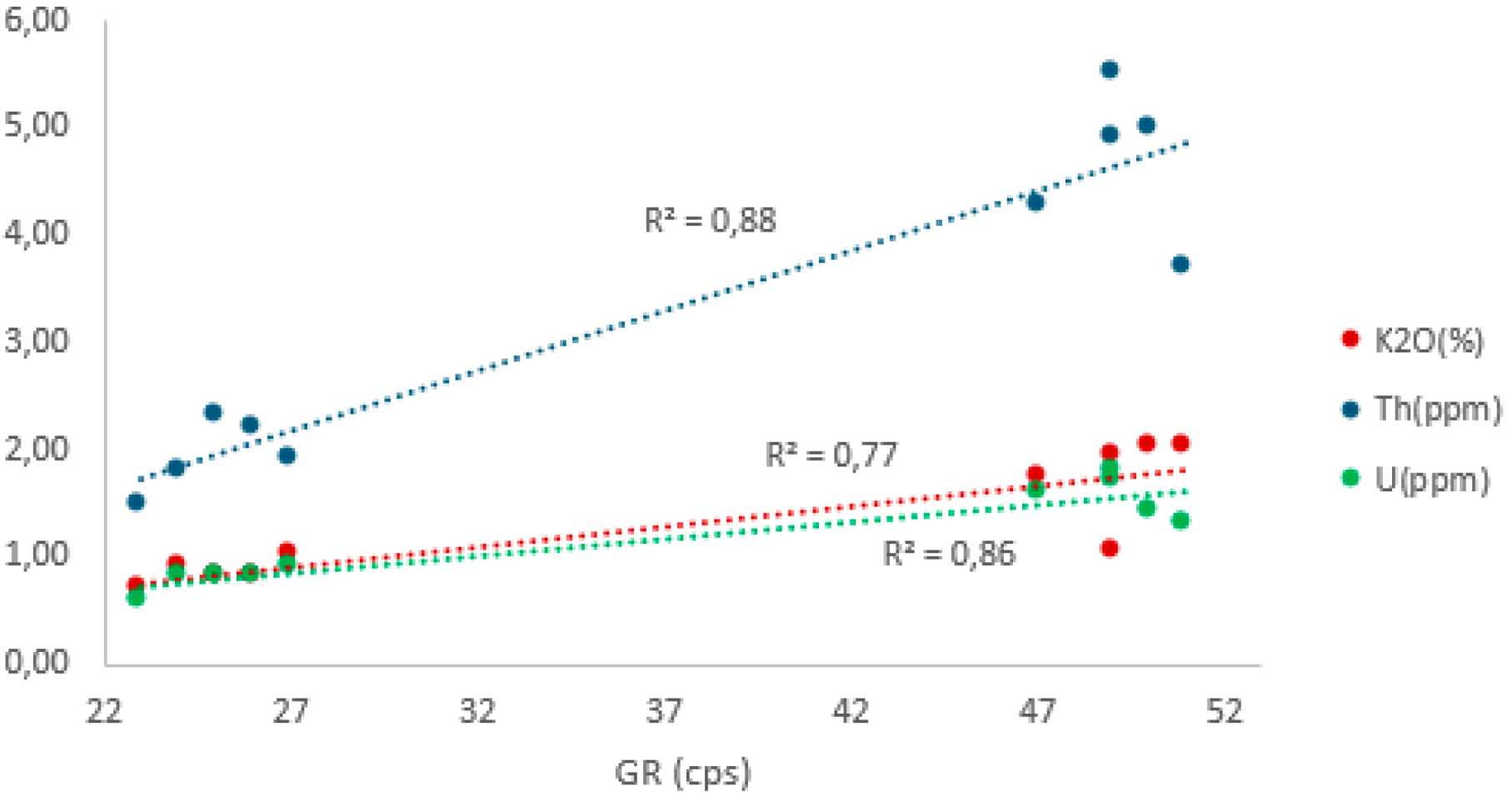

Figure 20. Correlation between Gamma-radiating elements and GR lectures. U and Th show the highest correlation with the GR values.

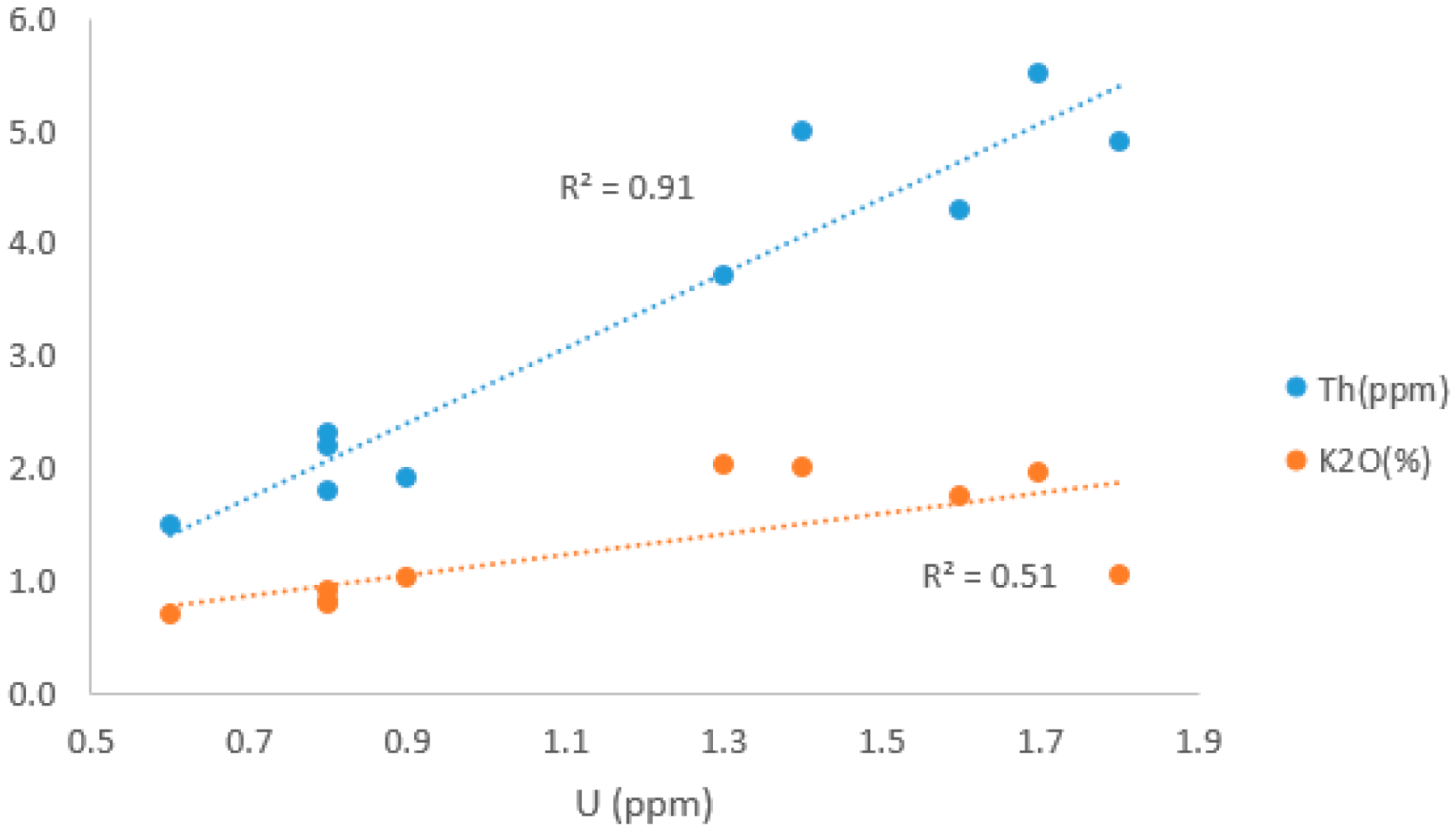

Figure 21. Correlation of Th and K with U. It is highly positive between U and Th, and medium positive between U and K.

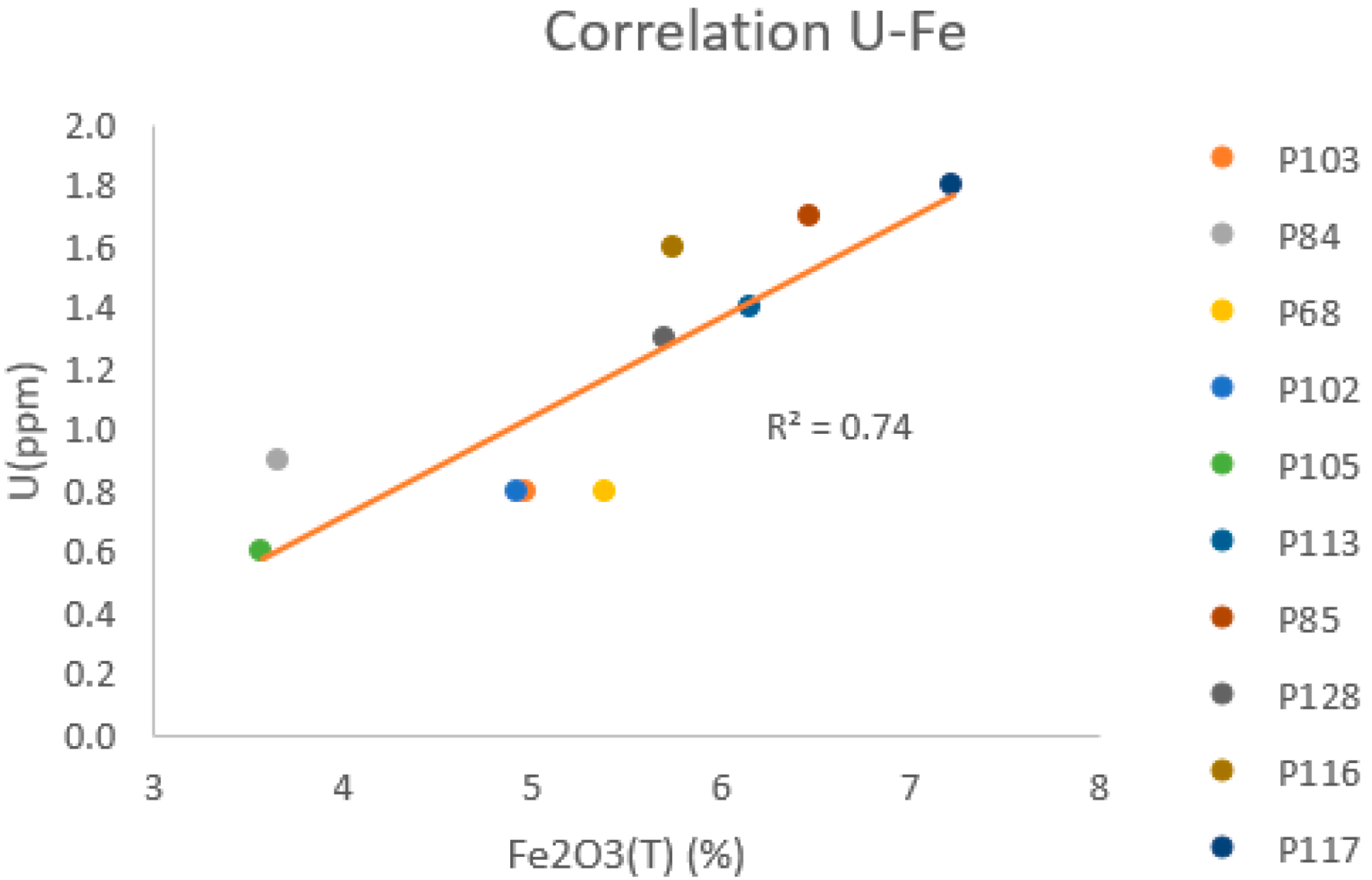

Figure 22. Positive correlation between U and Fe.

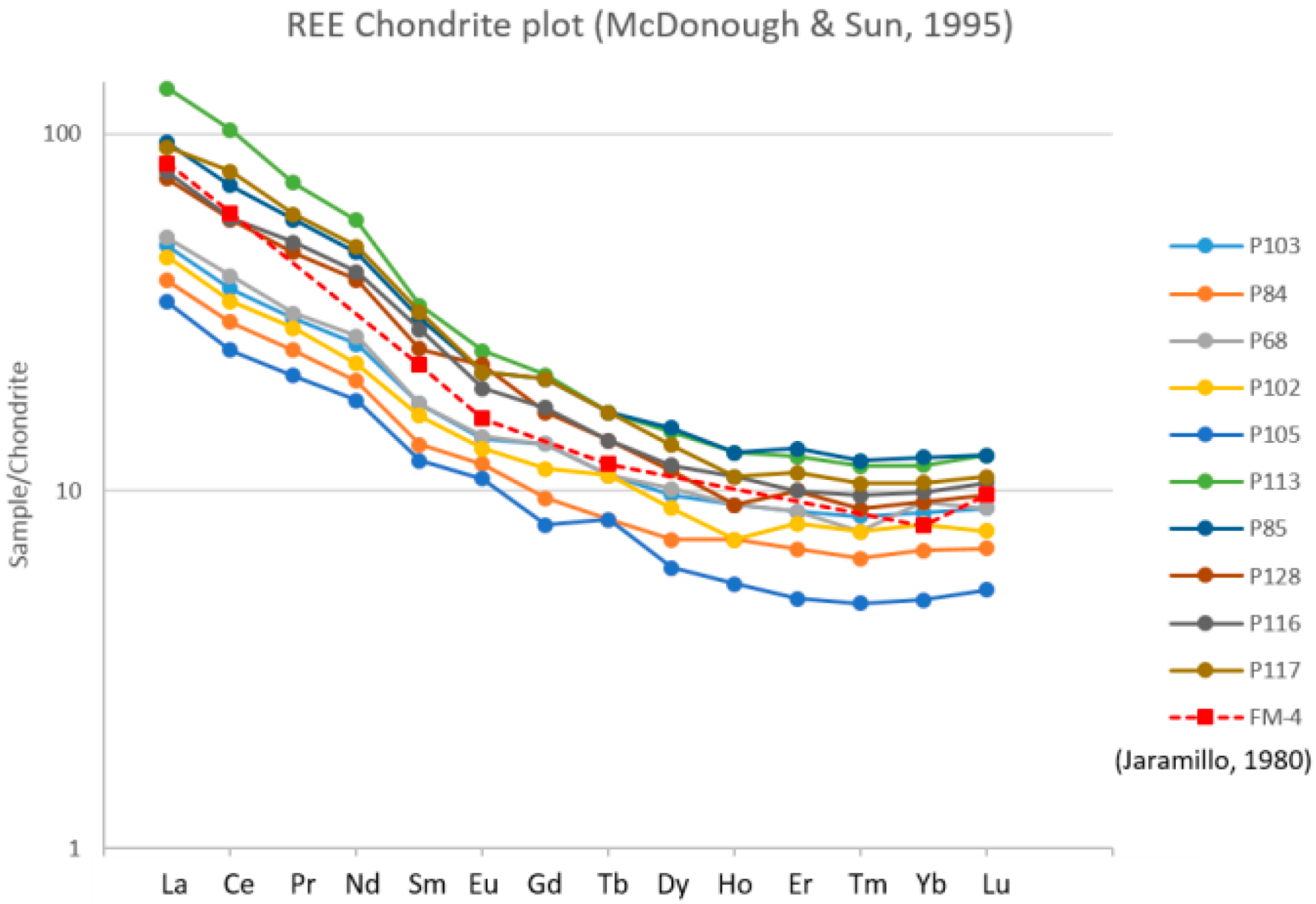

Figure 23. REE Chondrite plot (McDonough and Sun, 1995). Soil samples have the typical response of intermediate volcanic rocks, compared with andesite FM-4 studied by Jaramillo (1980).

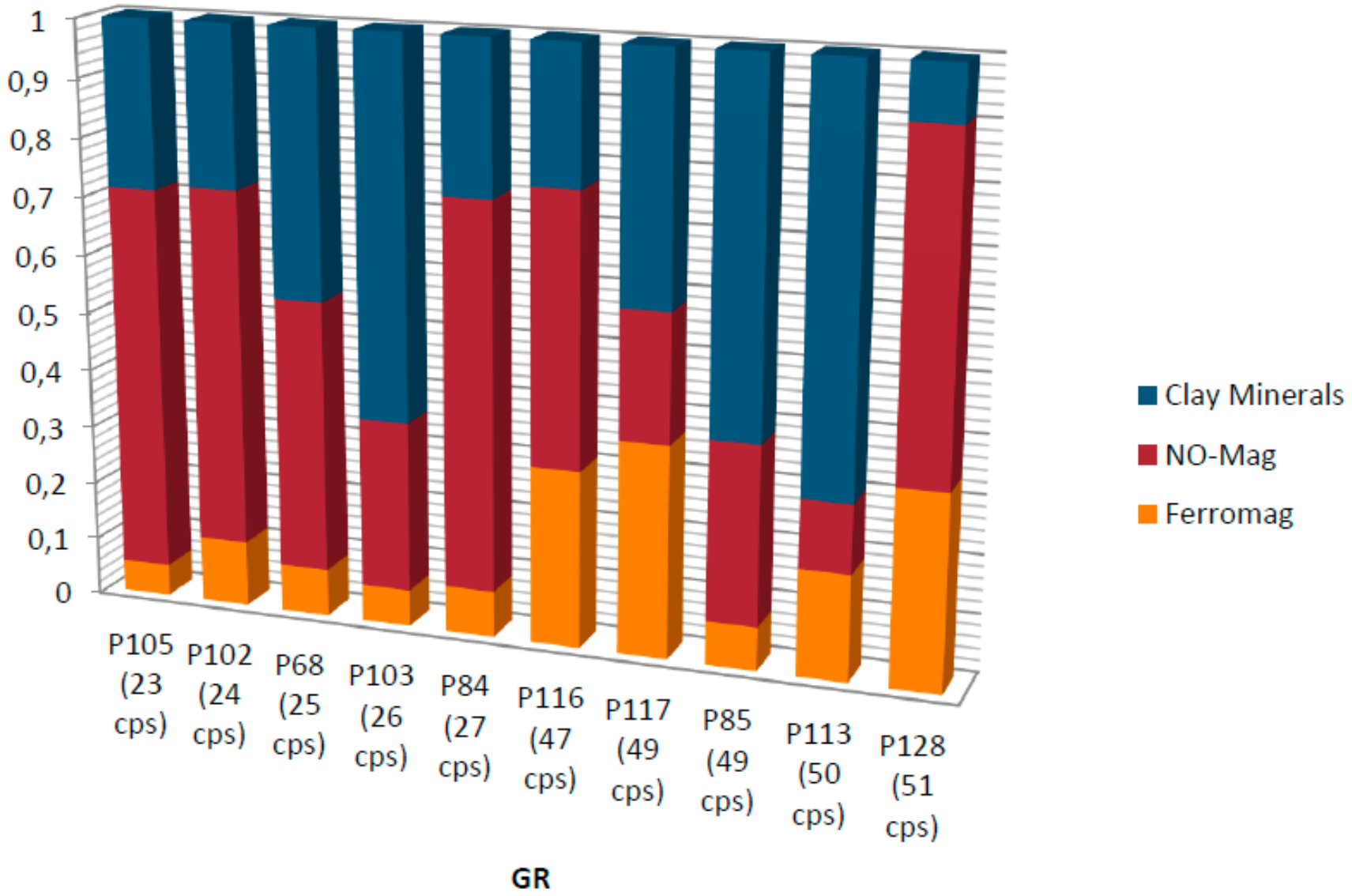

Figure 24. Ratios of clay minerals, no-magnetic minerals, and magnetic minerals for the soil samples, sorted by increasing GR. Magnetic content in the samples increases with GR values increases, while non-magnetic and clay minerals content have a significant variability over the samples.

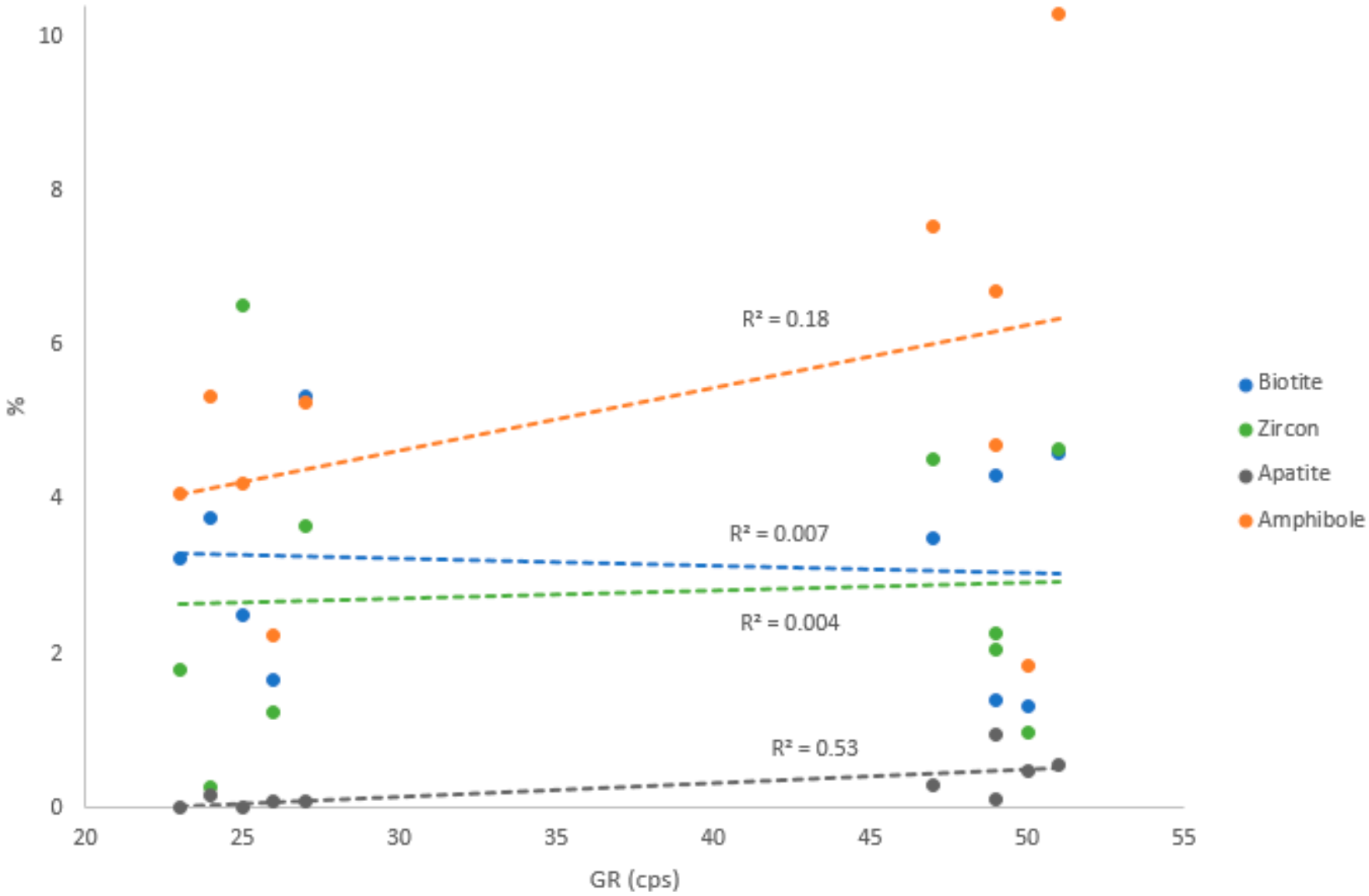

Figure 25. Correlation between GR values and minerals with Gamma-radiating elements. There is not a significant correlation between these minerals and the GR values.

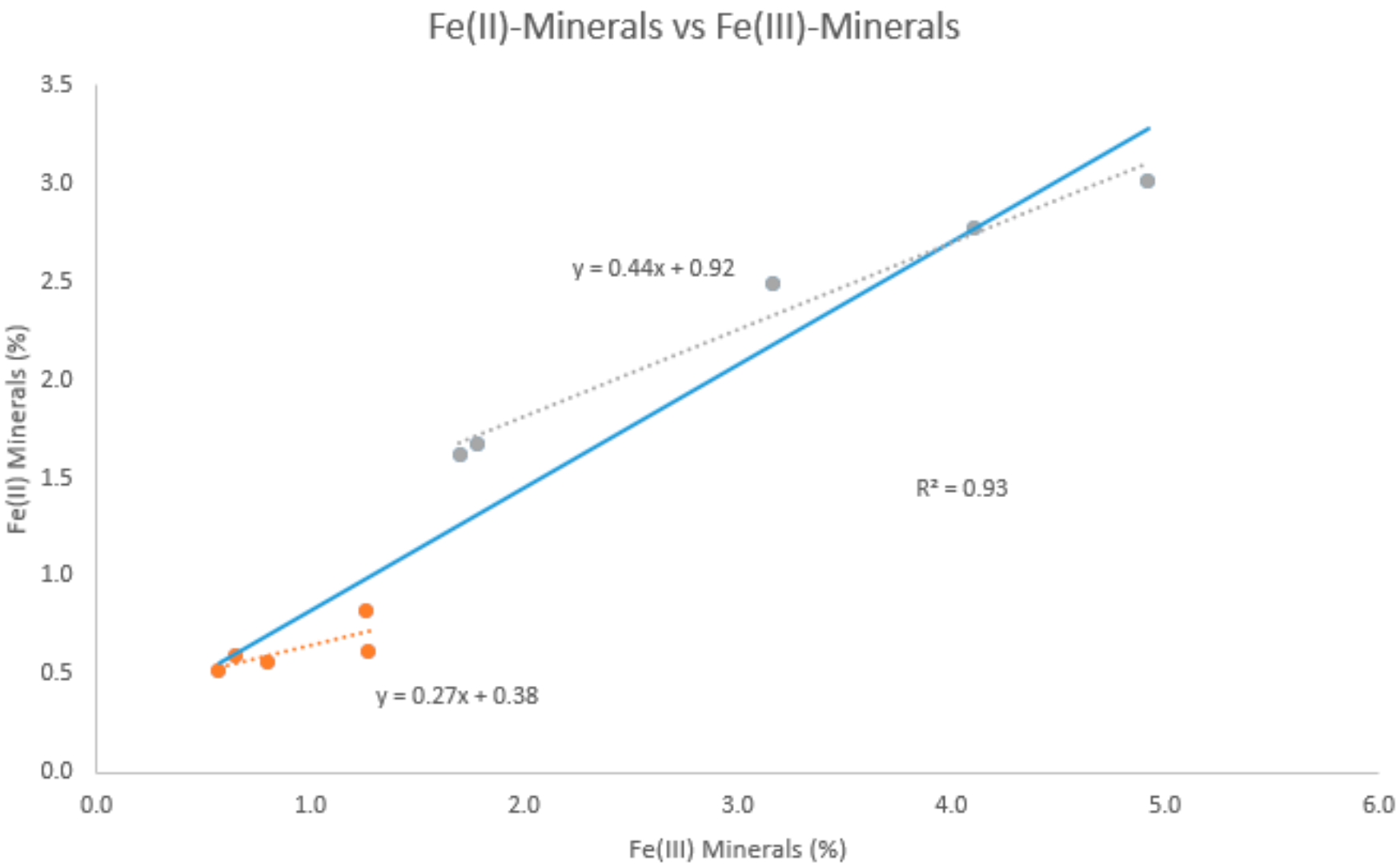

Figure 26. High positive correlation between Fe^{2+} and Fe^{3+} minerals. Fe^{3+} is reduced from Hematite and Goethite to produce Fe^{2+}, which led the authigenic formation of partially reduced Magnetite and reduced Ilmenite, Siderite and Ferroan-Dolomite. Fe^{2+}/Fe^{3+} ratio is higher for Fe^{3+} values more than 3%.

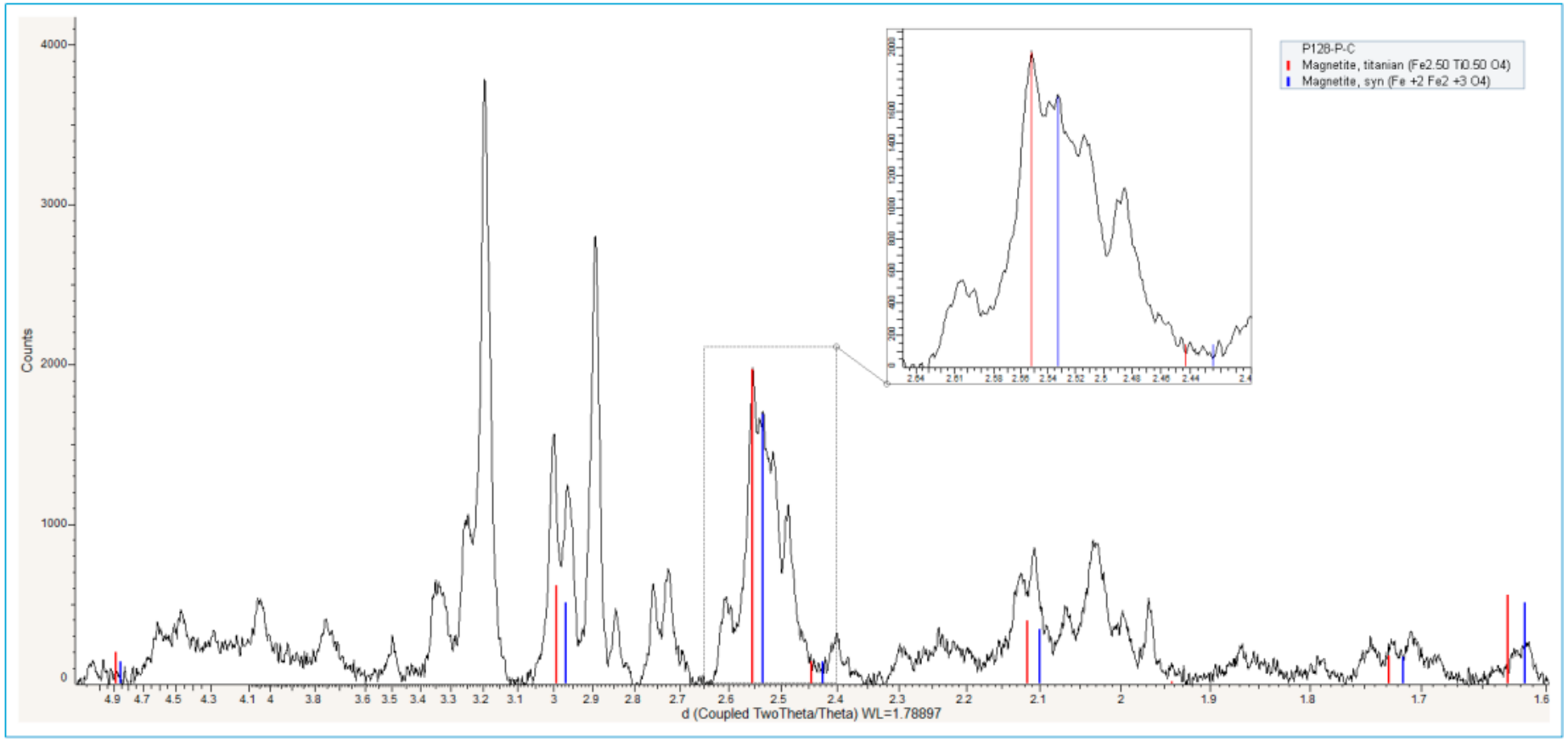

Figure 27. Diffractogram of the concentrated sample P128-P-C. Titanian magnetite (red) and stoichiometric magnetite (blue) are clearly distinguished (zoom in zone).

Figure 28. Cross-cutting section from the location of one of the sampled points. Different sedimentation events are identified, leading to mechanical differentiation of the materials that formed the soil.

Gamma-Radiation	131 points
Magnetic Field Strength	115 points
Soil samples	82 points

Table 1. Summary of the data and soil samples collected in the field.

Analyte Symbol	SiO2	Al2O3	Fe2O3(T)	MnO	MgO	CaO	Na2O	K2O	TiO2	P2O5	LOI	Total
Unit Symbol	%	%	%	%	%	%	%	%	%	%	%	%
Detection Limit	0.01	0.01	0.01	0.001	0.01	0.01	0.01	0.01	0.001	0.01		0.01
P103	65.74	11.7	4.96	0.061	1.35	2.17	1.15	0.81	0.527	0.03	11.9	100.4
P84	73.45	11.52	3.66	0.038	1.2	2.15	1.82	1.02	0.36	< 0.01	4.96	100.2
P68	67.42	11.83	5.39	0.086	1.67	2.6	1.53	0.79	0.59	0.04	7.99	99.93
P102	68.63	11.37	4.92	0.078	1.87	3.32	1.91	0.9	0.528	0.04	6.79	100.3
P105	74.31	9.89	3.57	0.047	1.16	2.17	1.73	0.7	0.333	< 0.01	5.38	99.26
P113	57.4	16.25	6.15	0.115	2.58	3.55	3.64	2.01	0.677	0.14	6.99	99.49
P85	58.88	15.67	6.47	0.118	2.37	3.18	2.28	1.96	0.812	0.09	7.49	99.31
P128	60.95	15.67	5.7	0.095	3.38	4.78	3.87	2.02	0.693	0.18	1.91	99.24
P116	63.01	15.48	5.74	0.089	2.27	3.82	3.63	1.74	0.659	0.13	3.99	100.6
P117	58	15.04	7.22	0.134	2.62	3.79	2.42	1.05	0.827	0.11	7.75	98.97

Table 2. Results from FUS-ICP for major elements.

Whole sample mineral composition estimated by XRD from magnetic and non-magnetic fractions (%)												
#	Mineral	P105	P102	P68	P103	P84	P116	P117	P85	P113	P128	Average
1	Quartz	40.8	28.5	23.2	20.1	35.1	11.9	8.3	8.6	2.5	9.0	18.8
2	Enstatite, ferroan	13.1	24.6	11.3	6.5	16.6	35.5	19.4	14.1	14.7	43.8	19.9
3	Andesine	4.8	6.3	3.4	2.1	-	6.6	8.1	3.1	4.2	9.1	5.3
4	Labradorite	-	-	-	-	5.7	-	-	-	-	-	5.7
5	Riebeckite	3.5	4.7	3.0	1.9	4.6	4.8	3.0	4.7	1.3	7.4	3.9
6	Zircon	1.8	0.3	6.5	1.2	3.6	4.5	2.1	2.3	1.0	4.7	2.8
7	Biotite	2.9	3.4	2.2	1.5	4.7	3.2	4.0	1.3	1.3	3.3	2.8
8	Augite	1.9	2.0	0.3	0.1	0.3	2.5	2.0	1.2	1.1	3.6	1.5
9	Hornblende, pargasitic	0.5	0.6	1.2	0.4	0.6	2.7	1.7	2.0	0.5	2.9	1.3
10	Rutile	0.8	0.3	1.1	0.7	1.3	0.8	3.6	-	0.9	1.3	1.2
11	Dolomite, ferroan	0.3	0.3	0.4	0.2	0.3	1.0	1.1	0.2	0.7	1.1	0.6
12	Goethite	0.1	0.2	0.1	0.1	0.1	0.8	1.8	-	0.2	0.6	0.5
13	Magnetite, titanian	0.1	0.3	0.6	0.2	0.2	0.8	1.1	0.1	0.5	0.9	0.5
14	Magnetite	0.1	0.2	0.6	0.1	0.2	0.7	0.8	0.1	0.4	0.7	0.4
15	Clorite	0.3	-	0.3	0.1	0.5	0.2	0.2	0.2	0.1	1.3	0.3
16	Apatite	-	0.2	-	0.1	0.1	0.3	0.9	0.1	0.5	0.6	0.3
17	Vermiculite	0.1	0.4	-	-	0.1	0.1	0.1	-	-	-	0.1
18	Ilmenite	-	-	-	-	-	-	-	0.1	-	-	0.1
19	Hematite	0.1	-	0.1	-	0.1	0.2	-	-	-	-	0.1
20	Siderite	0.1	-	-	-	-	-	-	0.1	-	-	0.1
	Total No-mag+mag	71.3	72.3	54.6	35.4	74.1	76.7	58.1	38.0	29.9	90.3	60.1
	Total clays	28.7	27.7	45.4	64.6	25.9	23.3	41.8	62.0	70.1	9.6	39.9
	Total	100.0	100.0	100.0	100.0	100.0	100.0	99.9	100.0	100.0	99.9	100.0
	GR	23	24	25	26	27	47	49	49	50	51	37

Table 3. Whole sample percentages of the minerals identified by XRD sorted vertically by decreasing average values in all samples, which are sorted horizontally by increasing GR measurements. The minerals found in the samples correspond to the typical association of andesitic rocks: intermediate composition Plagioclase (i.e. Andesine in nine samples and Labradorite in one), two Pyroxenes (i.e. mainly Ferroan Enstatite, and Augite in less proportion), two Amphiboles (i.e. Riebeckite and Pargasitic Hornblende), Biotite and its alteration products (i.e. Chlorite and Vermiculite), Zircon, Apatite, and Fe-Ti oxides/hydroxides (i.e. Magnetite, Ilmenite, Goethite, Hematite and Rutile). Two Magnetite species are identified: Titanian Magnetite is attributed to andesitic parental material from Nevado Del Tolima Volcano, and stoichiometric Magnetite is inferred to be authigenic. There are also identified Fe-bearing Carbonates in the soil samples (i.e. Ferroan-Dolomite and Siderite), which are inferred to be authigenic too. A significant variability in the composition of the soils is observed from the different proportion of each mineral in the samples.

Whole sample mineral composition estimated by XRD from magnetic and non-magnetic fractions (%)												
#	Mineral Classification	P105	P102	P68	P103	P84	P116	P117	P85	P113	P128	Average
1	Pyroxene (Enstatite+Augite)	15.0	26.6	11.6	6.6	16.9	38.0	21.4	15.3	15.9	47.4	21.5
2	Quartz	40.8	28.5	23.2	20.1	35.1	11.9	8.3	8.6	2.5	9.0	18.8
3	Plagioclase (Andesine/Labradorite)	4.8	6.3	3.4	2.1	5.7	6.6	8.1	3.1	4.2	9.1	5.3
4	Amphibole (Riebeckite+Pargasitic Hornblende)	4.1	5.3	4.2	2.2	5.3	7.5	4.7	6.7	1.8	10.3	5.2
5	Biotite (Biotite+Chlorite+Vermiculite)	3.2	3.7	2.5	1.7	5.3	3.5	4.3	1.4	1.3	4.6	3.2
6	Zircon	1.8	0.3	6.5	1.2	3.6	4.5	2.1	2.3	1.0	4.7	2.8
7	Fe-Ti Oxides/Hydroxides (Magnetite+Ilmenite+Goethite+Hematite+Rutile)	1.2	1.0	2.7	1.1	1.8	3.4	7.3	0.3	2.0	3.5	2.4
8	Carbonate (Ferroan-Dolomite+Siderite)	0.4	0.3	0.4	0.2	0.3	1.0	1.1	0.3	0.7	1.1	0.6
9	Apatite	-	0.2	-	0.1	0.1	0.3	0.9	0.1	0.5	0.6	0.3
	Total No-mag+mag	56.3	45.6	42.9	28.8	57.3	38.7	36.8	22.7	14.1	42.9	38.6
	Total clays	28.7	27.7	45.4	64.6	25.9	23.3	41.8	62.0	70.1	9.6	39.9
	Total	100.0	100.0	100.0	100.0	100.0	100.0	99.9	100.0	100.0	99.9	100.0
	GR	23	24	25	26	27	47	49	49	50	51	37

Table 4. Whole sample percentages of the classified minerals identified by XRD, sorted vertically by average values in all samples, which are sorted horizontally by GR values.